Teknomekanik, Vol. 9, No. 2, 2026, pp. 177-202
e-ISSN: 2621-8720 p-ISSN: 2621-9980

Component-wise exergy loss analysis under injection timing and EGR variations in a heavy-duty diesel engine

Eihab A. Raouf Mustafa

Department of Mechanical Engineering, College of Engineering, Qassim University, **Saudi Arabia**

*Corresponding Author: eomer@qu.edu.sa
Received: 14 February 2026; *Revised:* 30 April 2026; *Accepted:* 07 May 2026

Cite this https://doi.org/10.24036/teknomekanik.v9i2.54472

Abstract: This study investigates the component-wise exergy behavior of a heavy-duty diesel engine under combined variations in injection timing and exhaust gas recirculation (EGR). A calibrated Diesel-RK model was used to simulate steady-state operation over a representative speed-load range. Fuel, brake, exhaust, wall heat, and destruction exergy terms were then evaluated using a consistent post-processing framework. The results showed that increasing EGR from 0 to 0.20 reduced the brake exergy fraction from 33% to 14%. In comparison, the destruction fraction increased from 44% to 73%, indicating that dilution intensified combustion-related irreversibility with a greater influence on irreversibility than on wall heat transfer. Across the investigated speed-load range without EGR, destruction typically remained within about 39–45% of fuel exergy. Advancing injection timing shifted heat release toward top dead center and redistributed wall heat exergy from the liner (40% to 26%) toward the piston and cylinder head, with contributions increased to approximately 37–40% each. At high load, moderate advancement improved thermodynamic efficiency, whereas excessive advancement increased wall thermal loading and reduced further gains. At part load, sensitivity increased because combustion duration appeared to influence thermal response more strongly than peak temperature. A limited trade-off region was identified in which exergy efficiency exceeded about 30%, and destruction dropped below roughly 45%, primarily at advanced timing and high load. However, excessive injection advancement resulted in physically infeasible EGR operation due to insufficient exhaust pressure to sustain recirculation flow, thereby defining a practical operating boundary. Injection timing affected not only efficiency but also whether EGR could function, therefore, optimal calibration must balance combustion phasing, dilution-induced irreversibility, and component-level thermal loading.

Keywords: combustion irreversibility; diesel engine; exergy analysis; exhaust gas recirculation; injection timing

1. Introduction

Internal combustion engines convert the chemical energy of fuel into mechanical power through combustion-driven thermodynamic processes [1]. The chemical energy of fuel is first converted to thermal energy by means of combustion of fuel with oxygen from the air, which occurs within the cylinder of the engine [2]. The thermal energy raises the pressure and temperature of the gases within the engine, and the high-pressure gas then expands against the mechanical mechanism of the engine [3]. During diesel engine operation, air is compressed, fuel is injected, and combustion increases in-cylinder pressure, thereby driving piston motion [4]. However, not all released energy is converted into useful work; a significant fraction is rejected through exhaust gases or transferred to combustion chamber walls [5]. Diesel engines operate by compression ignition, in which fuel is injected into compressed air and combustion occurs without spark assistance [6]. Consequently, the higher compression ratio gives diesel engines higher thermal efficiency than spark-ignition engines.

Diesel engines are widely used in heavy-duty and industrial systems [7]. Elevated in-cylinder pressure and temperature intensify heat transfer to the piston crown, cylinder head, and liner [8]. Injection timing and exhaust gas recirculation (EGR) are widely employed to regulate combustion and emissions [9]. Injection timing refers to the crank-angle at which fuel injection begins relative to top dead center. It governs combustion phasing within the engine cycle [10]. Advancing injection timing shifts combustion closer to top dead center (TDC), generally increasing peak pressure and temperature [11]. Conversely, retarding injection shifts heat release later in the cycle and reduces peak pressure [12].

Variations in injection timing alter ignition delay, heat-release characteristics, and in-cylinder pressure evolution. Consequently, work output, exhaust temperature, and wall heat transfer are affected. For this reason, injection timing is treated as a primary calibration parameter during diesel engine calibration [13]. Advancing or retarding injection timing modifies piston position, in-cylinder pressure, and local temperature conditions at injection, thereby influencing ignition delay, fuel–air mixing, and combustion behavior [14]. Accordingly, injection timing has been widely investigated to optimize low-temperature combustion strategies aimed at reducing pollutant emissions [15]. Diesel engines pose major problems due to their higher emissions of oxides of nitrogen (NOx) and particulate matter (PM) [16]. The major constituents of diesel exhaust include carbon dioxide (CO_2), water vapor (H_2O), nitrogen (N_2), oxygen (O_2), carbon monoxide (CO), hydrocarbons (HC), oxides of nitrogen (NO_x), and particulate matter (PM) are present in smaller but environmentally significant quantities. Exhaust Gas Recirculation is an effective method for NOx control. The exhaust gases mainly consist of carbon dioxide, nitrogen, and residual species. and the mixture has a higher specific heat compared to atmospheric air [17]. Part of the exhaust flow can be redirected to the intake to dilute the fresh charge [18]. This reduces oxygen concentration within the cylinder and lowers combustion temperature. As the dilution level increases, pressure development and heat-release characteristics change [19]. The impact extends beyond NOx reduction, affecting combustion stability, efficiency, and heat transfer. For this reason, the EGR rate is treated as a tuning variable rather than a fixed operating condition [20].

Conventional energy analysis shows how much energy enters and leaves the engine [21]. However, energy balances do not distinguish between useful and degraded energy forms [22]. Exergy analysis evaluates the usable work potential of fuel rather than its total energy content [23]. In diesel operation, only part of the fuel exergy is converted into brake work. The remainder leaves with the exhaust gases or is lost through wall heat transfer and combustion-related irreversibilities [24]. Expressing these losses in exergy terms makes thermodynamic degradation explicitly quantifiable [25].

Numerous studies have examined injection timing and exhaust gas recirculation (EGR) in diesel engines. In most cases, the analysis has been limited to overall engine responses, including brake thermal efficiency, fuel consumption, and regulated emissions. It is generally recognized that EGR reduces peak combustion temperatures and, consequently, NOx formation. Likewise, changing the start of injection alters the rate of heat release and the development of in-cylinder pressure. These relationships are not new; they have been reported and discussed repeatedly in previous experimental and numerical investigations. However, most of these works evaluate the engine as a single thermodynamic unit. As a result, they provide limited information on how irreversibilities and heat-related losses are redistributed among individual combustion chamber components as injection timing and dilution levels vary.

In much of the available literature, exergy analysis of diesel engines is carried out at the overall engine level. Researchers typically report total exergy destruction and overall exergy efficiency without separating the contributions of specific combustion chamber components. Although this approach is useful for judging the second-law performance of the engine as a single system, it does

not explain where and how the losses actually occur inside the cylinder. The heat transfer paths and sources of irreversibility at the piston, cylinder head, and liner are therefore treated collectively rather than individually. As a result, the effects of injection timing and EGR on the exergy losses associated with each surface have not been examined in sufficient detail. Studies that explicitly couple EGR effects with a component-wise interpretation of exergy losses are notably scarce, especially for heavy-duty diesel engines operating over realistic speed–load ranges.

This limitation is more pronounced in heavy-duty engines, which often operate for long periods at high load and under severe thermal conditions. In such regimes, heat transfer to the combustion chamber walls and the associated exergy losses are significant contributors; they directly influence overall efficiency and the thermal stress experienced by critical components. The piston crown, cylinder head, and liner are continuously exposed to high temperatures and pressure gradients, making the distribution of thermal loads a practical concern for durability. Without a component-wise exergy assessment, it becomes difficult to relate changes in combustion control, such as injection timing or EGR, to the way thermal and irreversibility-related loads are redistributed within the chamber. Despite these advances, the localized thermodynamic impact of combustion control strategies, particularly the combined influence of injection timing and EGR, on the redistribution of exergy losses within the piston, cylinder head, and liner remains insufficiently understood. This limitation is especially relevant for heavy-duty diesel engines, where thermal loading and durability are directly linked to the spatial distribution of heat transfer and irreversibility. In particular, previous studies have not systematically resolved how exergy losses are redistributed among individual combustion chamber components under coupled variations of injection timing and EGR across realistic operating conditions. Therefore, the present study addresses this gap by providing a component-wise exergy analysis under coupled variations of injection timing and EGR across a representative speed–load range. Unlike conventional approaches, the analysis resolves the wall-related exergy losses at the level of individual combustion chamber components, enabling a physically grounded interpretation of how combustion phasing and charge dilution redistribute thermal and irreversibility pathways within the engine.

Based on these considerations, the present work investigates the combined influence of injection timing and EGR on the distribution of exergy losses among the main combustion chamber components of a heavy-duty diesel engine. The analysis distinguishes the exergy losses attributable to the piston, cylinder head, and liner individually, rather than evaluating the engine as a single, undivided control volume. The aim is to quantify how variations in injection phasing and dilution level modify the location and magnitude of irreversibilities within the chamber. By relating these component-level results to the overall engine performance trends, the study seeks to clarify how combustion control strategies affect both efficiency and thermal loading. This integrated view provides a more physically grounded basis for selecting injection and EGR settings in heavy-duty applications, where performance, durability, and thermal management must be considered together.

2. Material and methods

2.1 Engine specifications and reference operating configuration

The present investigation was conducted on a turbocharged, direct-injection heavy-duty diesel engine used in commercial truck applications. A six-cylinder, four-stroke configuration with a common-rail injection system and bowl-in-piston combustion chamber was considered. In service, the engine operates over a wide speed–load range and may run at high load for extended periods. The principal geometric and operating specifications, including bore, stroke, compression ratio, and displacement, are summarized in Table 1. The baseline operating condition was defined at zero EGR with a reference start of injection (SOI) calibrated to reproduce nominal brake torque and thermal efficiency.

Table 1. Main specifications of the reference engine (Mercedes-Benz OM457)

Item	Description	Item	Description
Engine type	Heavy-duty DI diesel	Max power	260 kW at 2000 rpm
Number of cylinders	6-cylinder, In-line	IVO / IVC	17° BTDC / 50° ABDC
Valve mechanism	24-valve, Gear Drive	EVO / EVC	50° BBDC / 13° ATDC
Combustion Chamber	DI bowl-in-piston	Injection timing (SOI)	9° BTDC
Fuel system	Direct injection	Injection duration	3 ms
Displacement	12 liters	Nozzle hole diameter	≈ 0.20 mm
Bore × Stroke	128 mm × 155 mm	Injection system	Direct injection
Compression ratio	17.5:1	Number of nozzle holes	7
Turbocharger pressure ratio	1.50 ⟶ 3.0 (rated = 2.9)	Ambient parameters	P_0 = 1 bar, T_0 = 313 K
Max torque	1600 N.m at 1100 rpm	Connecting rod length	287 mm

2.2 Numerical model and simulation framework

Engine simulations were performed using the Diesel-RK simulation platform, in which in-cylinder thermodynamics were calculated with a zero-dimensional, single-zone combustion model incorporating sub-models for injection, heat release, gas exchange, and wall heat transfer. Heat transfer to the piston crown, cylinder head, and liner was evaluated using embedded wall heat-transfer correlations, while combustion evolution was represented by calibrated empirical sub-models that accounted for injection-rate shaping, ignition delay, spray dynamics, and mixing-controlled combustion behavior. The analysis used an energy-based formulation governed by mass and energy conservation during the closed-cycle period, and cylinder pressure was obtained from thermodynamic state equations that accounted for combustion heat release and wall heat transfer. Gas properties were treated as temperature-dependent, and each operating condition was iterated until convergence in pressure trace, brake power, and heat-transfer characteristics was achieved. The framework provides the in-cylinder pressure, temperature, and heat-release rate as functions of crank angle under steady-state operating conditions.

The model has been used in diesel engine studies for performance prediction, fuel consumption estimation, combustion and emission analysis, and the optimization of injection strategy, EGR, valve timing, and turbocharging systems. In addition, it has been extended to dual-fuel combustion analysis and integrated with external optimization platforms for parametric studies.

2.3 Model calibration procedure

The numerical model was calibrated to reproduce the reference engine operating characteristics. Fuel mass per cycle was adjusted at each speed–load point to achieve the target brake torque. Calibration ensured agreement among brake power, torque, and brake thermal efficiency. The injection duration under baseline conditions was derived from the calibrated fuel mass and the injection rate profile. The reference SOI was defined as the nominal operating point and used as the baseline for comparison in the parametric study. The load definition and the corresponding fuel mass per cycle are summarized in Table 2.

Table 2. Load definition and corresponding fuel injection quantities at various engine speeds

Engine speed (rpm)	Load (%)	Target Torque (N·m)	Fuel Mass per Cycle (g/cycle)
1000	50	797	0.11
	100	1593	0.22
1100 (Reference)	50	806	0.11
	100	1612	0.22
2000	50	776	0.11
	100	1552	0.22
3000	50	712	0.115
	100	1423	0.23

Model validation was performed at the reference operating condition by comparing the simulated brake torque, peak in-cylinder pressure, and brake thermal efficiency with corresponding engine specifications and data reported in the literature for similar heavy-duty diesel engines. The predicted values showed good agreement within the typical uncertainty range of one-dimensional diesel engine simulations, confirming that the model captures the main thermodynamic trends with sufficient accuracy for parametric analysis. Following validation, all model parameters were kept constant, and only injection timing and EGR rate were varied to isolate their effects on exergy distribution.

2.4 Operating conditions and parametric matrix

Three engine speeds were selected, and at each speed, simulations were carried out at 50% and 100% load. The start of injection (SOI) was varied over a specified crank-angle range before top dead center. Exhaust gas recirculation (EGR) was introduced at selected recirculation rates. For each speed–load point, all combinations of SOI and EGR were evaluated, forming the parametric matrix of the study. All simulations were performed under steady-state conditions. The complete operating matrix is summarized in Table 3.

Table 3. Operating matrix for the Diesel-RK simulation campaign

Engine Speed (rpm)	Load (% of Full Torque)	SOI (°BTDC)	EGR Rate (%)	Number of simulation Cases
1000, 2000, 3000	50 and 100	0, 3, 6, 9, 12, 15, 18	0, 10, 20	126

The operating matrix consisted of 126 simulation cases generated by combining three engine speeds, two load conditions, seven SOI settings, and three EGR rates. The procedure began with model calibration at the baseline condition. The speed–load operating points were then defined, followed by variations in injection timing and EGR. Thermodynamic and heat-transfer variables were extracted for each case, and the corresponding component-wise exergy calculations were performed. To ensure methodological clarity, the study follows a structured simulation-based framework. The calibrated and validated model is extended across the defined speed–load operating points, in which injection timing and EGR rate are systematically varied to construct the parametric matrix. Subsequently, post-processing is applied to compute component-wise exergy terms and evaluate their distribution under each operating condition. This approach ensures that the observed variations in exergy behavior are directly attributable to the controlled input parameters.

2.5 Extraction of component-wise wall heat transfer

For each simulated operating case, the instantaneous and cycle-averaged heat-transfer rates to the piston crown, cylinder head, and liner were extracted directly from the simulation output. The software provides separate wall heat-transfer terms for each component. The cycle-averaged heat-transfer rate for each surface was converted to power units (W). These values were used as the basis for the component-wise exergy calculations. Wall temperatures for each component were obtained from the model outputs and treated as uniform mean surface temperatures over the cycle.

2.6 Exergy formulation and balance equations

The exergy analysis was performed using a reference environment defined by ambient temperature (T_0) and pressure (p_0). Fuel chemical exergy was calculated from the lower heating value using a standard exergy-to-energy ratio for diesel fuel. An exergy-based framework was employed to evaluate the generation of irreversibility and clarify how the fuel's useful work potential is degraded under different operating conditions. This formulation enables direct linkage between combustion-driven heat release and spatially resolved exergy losses across chamber components. For each simulated case, the fuel exergy rate was calculated from the fuel mass flow rate and the corresponding specific chemical exergy. Based on this framework, the engine exergy balance was formulated by accounting for the useful brake work output and the main loss pathways, namely exhaust exergy, heat-transfer losses, and internal exergy destruction from irreversible processes. The resulting overall exergy balance can therefore be expressed as in Equation (1).

$$\dot{E}x_{fuel} = \dot{E}x_{work} + \dot{E}x_{exh} + \dot{E}x_{wall} + \dot{E}x_{dest} \quad (1)$$

where $\dot{E}x_{fuel}$ denotes the rate of fuel exergy supplied to the engine, $\dot{E}x_{work}$ represents the useful brake work exergy, $\dot{E}x_{exh}$ corresponds to the exergy carried by the exhaust gases, $\dot{E}x_{wall}$ accounts for the exergy associated with heat-transfer losses to the surroundings, and $\dot{E}x_{dest}$ quantifies the exergy destruction resulting from internal irreversibilities. The exergy input rate to the engine due to mass transfer consisted of the chemical exergy rate of the fuel and that of the combustion air. However, the contribution of the combustion air exergy may be neglected if the air is assumed to enter the engine at ambient conditions. The chemical exergy rate of the fuel is calculated as in Equation (2).

$$\dot{E}x_{fuel} = \dot{m}_f . \beta . LHV \quad (2)$$

where $\dot{E}x_{fuel}$ is the chemical exergy rate of fuel (kW), LHV is the low heat value of fuel kJ/kg, and β is the fuel chemical exergy factor (1.04 – 1.07). The physical exergy of exhaust gases is calculated as in Equation (3).

$$\dot{E}x_{exh} = \dot{m}_{exh}\left[cp(T_{exh} - T_0) - T_0\left(cp \ln\frac{T_{exh}}{T_0} - R \ln\frac{p_{exh}}{p_0}\right)\right] \quad (3)$$

The exhaust gases were assumed to behave as an ideal gas, and constant thermophysical properties were assumed for the exhaust gases, with R_0 = 0.287 kJ/kg K, and cp = 1.16 kJ/kg K evaluated at the exhaust temperature. The useful work exergy was taken equal to the brake power output, as shown in Equation (4).

$$\dot{E}x_{work} = BP \quad (4)$$

The exergy associated with heat transfer is calculated using Equation (5).

$$\dot{E}x_{wall} = \left(1 - \frac{T_0}{T_b}\right) \dot{Q}_{wall} \tag{5}$$

where T_0 is the ambient temperature and T_b is the boundary temperature at which heat transfer occurs. This formulation is derived from classical exergy theory. The boundary temperature T_b was taken as the average temperature of the corresponding heat-transfer sink (coolant or oil), as reported directly by the Diesel-RK outputs. The total wall heat transfer rate $\dot{Q}_{wall}$ was reconstructed by summing the heat flow rates to the cylinder head ($\dot{q}_{head}$), piston ($\dot{q}_{piston}$), and liner $\dot{q}_{liner}$ reported by Diesel-RK on a per-cylinder basis. The resulting value was then converted to the total engine wall heat loss and expressed in kW, as stated in Equation (6).

$$\dot{Q}_{wall} = \frac{N_{cyl}}{1000} (\dot{q}_{liner} + \dot{q}_{piston} + \dot{q}_{head}) \tag{6}$$

where N_{cyl} number of cylinders. The overall wall heat exergy loss is defined as the sum of the exergy rates associated with heat transfer to the cylinder head, piston, and liner, and is expressed as in Equation (7).

$$\dot{E}x_{wall} = \dot{E}x_{heat,head} + \dot{E}x_{heat,piston} + \dot{E}x_{heat,liner} \tag{7}$$

To describe how the fuel exergy input was distributed among the main pathways, the exergy fractions were defined as in Equation (8).

$$\psi_{work} = \frac{\dot{E}x_{work}}{\dot{E}x_{fuel}}, \quad \psi_{exh} = \frac{\dot{E}x_{exh}}{\dot{E}x_{fuel}}, \quad \psi_{heat} = \frac{\dot{E}x_{wall}}{\dot{E}x_{fuel}}, \quad \psi_{dest} = \frac{\dot{E}x_{dest}}{\dot{E}x_{fuel}} \tag{8}$$

These fractions satisfy the normalization condition given in Equation (9).

$$\psi_{work} + \psi_{exh} + \psi_{wall} + \psi_{dest} = 1 \tag{9}$$

Finally, the exergy efficiency was defined as in Equation (10).

$$\eta_{ex} = \frac{\dot{E}x_{work}}{\dot{E}x_{fuel}} \tag{10}$$

To identify the contribution of individual combustion chamber components to thermodynamic irreversibilities, the exergy associated with wall heat transfer was resolved at the component level. The total wall heat transfer was decomposed into contributions from the cylinder head, piston, and liner, as reported by the simulation model on a per-cylinder basis. For each component i, the wall-related exergy loss was calculated as in Equation (11).

$$\dot{E}x_{wall,i} = \dot{Q}_{wall.i} \left(1 - \frac{T_0}{T_{b,i}}\right) \tag{11}$$

where T_0 is the ambient reference temperature, $T_{b,i}$ is the representative boundary temperature of the corresponding heat transfer sink, and $\dot{Q}_{wall.i}$ is the heat transfer rate to component i. The total

wall-related exergy loss was obtained by summing the contributions of the individual components and scaling the per-cylinder values to the full engine. This wall-resolved formulation enables a direct comparison of the relative importance of head-, piston-, and liner-related irreversibilities and their sensitivity to variations in injection timing.

To quantify the relative contribution of each combustion chamber wall component to the total wall-related exergy loss, normalized wall-exergy partition coefficients are defined by normalizing the heat-transfer exergy associated with the head, piston, and liner by the total wall heat exergy. These coefficients are expressed as in Equation (12).

$$\phi_{head} = \frac{\dot{E}x_{heat,head}}{\dot{E}x_{heat}}, \quad \phi_{piston} = \frac{\dot{E}x_{heat,piston}}{\dot{E}x_{heat}}, \phi_{liner} = \frac{\dot{E}x_{heat,liner}}{\dot{E}x_{heat}} \tag{12}$$

By definition, the sum of the component-wise wall heat exergy fractions equals the total wall heat exergy fraction, as defined in Equation (13).

$$\phi_{head} + \phi_{piston} + \phi_{liner} = 1 \tag{13}$$

2.7 Assumptions and limitations

The analysis assumes steady-state engine operation. Combustion was modeled using a single-zone approach, which does not explicitly resolve spatial temperature gradients within the combustion chamber. Wall temperatures were treated as mean values for each component. Radiation heat transfer was not modeled separately. Mechanical friction exergy destruction was not decomposed into its components. Despite these simplifications, the adopted framework enables consistent comparison of component-wise exergy trends under systematic variations in injection timing and EGR.

3. Results and discussion

The numerical outputs were extracted from the calibrated Diesel-RK simulations for each operating condition. Key performance and thermodynamic variables, including speed, load, fuel mass per cycle, exhaust conditions, and component-wise heat-transfer rates, were recorded without post-filtering. The raw datasets are presented in Tables A1-a–A1-c in the Appendix and are organized by engine speed. Exergy parameters were subsequently calculated through structured post-processing of the extracted simulation data. Fuel exergy input, brake exergy, exhaust exergy, wall heat exergy, and total exergy destruction were evaluated consistently across the full speed–load matrix. The calculated exergy results are presented in the Appendix in Tables A2-a, A2-b, and A2-c, arranged by engine speed and covering all injection timing and EGR variations considered in this study. The observed variations in exergy distribution can be interpreted through two coupled physical mechanisms: combustion phasing relative to top dead center (TDC), which governs the spatial distribution of heat release, and mixture reactivity under dilution, which controls the rate of entropy generation and irreversibility.

3.1 Baseline exergy balance and component-wise distribution

Figure 1(a) and 1(b) present a comparison of the baseline exergy balance at 2000 rpm and full load under the same injection timing (SOI = 9° BTDC) but with different EGR levels. In the baseline condition without EGR (Figure A), approximately one-third of the fuel exergy is converted into brake work (32.7%), while 19.4% leaves with the exhaust, and 4.0% is associated with wall heat transfer.

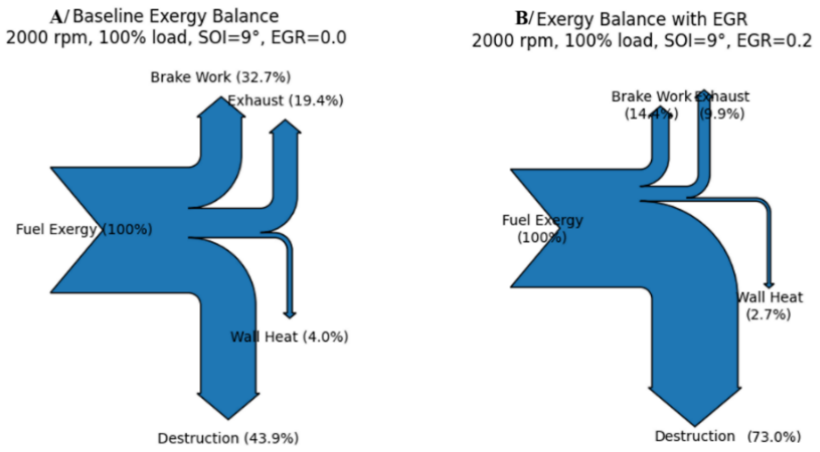

Figure 1. Comparison of the exergy balance at 2000 rpm and full load for EGR = 0.0 (a) and 0.2 (b) at a fixed injection timing (SOI = 9° BTDC)

The remaining fraction, about 43.9%, is destroyed due to internal irreversibilities during combustion and mixing. The increase in exergy destruction is linked to the reduction in oxygen partial pressure and the associated slowdown in reaction kinetics, suggesting increased mixing-related irreversibility rather than heat-transfer-driven losses. Similar behavior has been reported in the literature, where EGR-induced dilution limits oxygen availability and delays the combustion process, resulting in greater entropy generation and a corresponding rise in exergy destruction, particularly at high-load operation [26], [27].

When EGR is increased to 0.20 (Figure 1(b)), a marked redistribution of exergy is observed. The brake work fraction decreased significantly to 14.4%, and exhaust exergy was reduced to 9.9%, whereas exergy destruction increased sharply to 73.0%. Wall heat exergy decreases slightly to 2.7%. This change is small compared with the pronounced rise in exergy destruction, which becomes the dominant term in the balance. The results therefore indicate that, at this operating condition, the primary impact of EGR is reflected in increased internal irreversibilities rather than in a shift toward wall-related thermal losses. This comparison suggests the strong thermodynamic penalty associated with high EGR rates under full-load operation, where combustion remains mixing-controlled. The complete numerical exergy balance and component-wise fractions for all investigated speed–load and injection settings are reported in the Appendix (Table A2).

Figure 2 shows how the exergy fractions are distributed over the investigated speed–load range at a fixed injection timing of 9° BTDC for two EGR levels, 0.00 and 0.20. When EGR is not applied, the overall exergy balance remains relatively stable from one operating point to another. The brake work fraction remains in a relatively narrow band, typically around 33–35% at low and medium speeds, with a slight reduction as speed increases. In parallel, exergy destruction remains within the range of 39–45%, consistently representing the largest portion of the balance. This indicates that, even without EGR, internal irreversibilities associated with combustion and mixing processes dominate the thermodynamic losses across the examined operating conditions.

When EGR is increased to 0.20, a clear redistribution of exergy is observed. At 2000 rpm and full load, for example, brake work decreased from about 33% to 14%, while exergy destruction increased markedly from roughly 44% to 73%. A similar trend is observed at 3000 rpm and full load. Under EGR = 0.20, the destruction term rises sharply and reaches about 73–74%, while the share of useful brake work decreases accordingly. In contrast, the wall heat fraction remained relatively small in both EGR cases, typically between 3% and 7%, and varies only slightly compared with the pronounced increase in exergy destruction. This indicates that the main impact of EGR at

high-load operation is reflected in internal irreversibilities rather than in a significant shift toward wall-related thermal losses. The figure highlights the strong sensitivity of the overall exergy balance to EGR under high-load conditions, whereas part-load points show comparatively moderate shifts. For completeness, the detailed numerical exergy fractions for all simulated operating points and injection settings, including cases not explicitly visualized in this figure, are reported in the Appendix (Table A2).

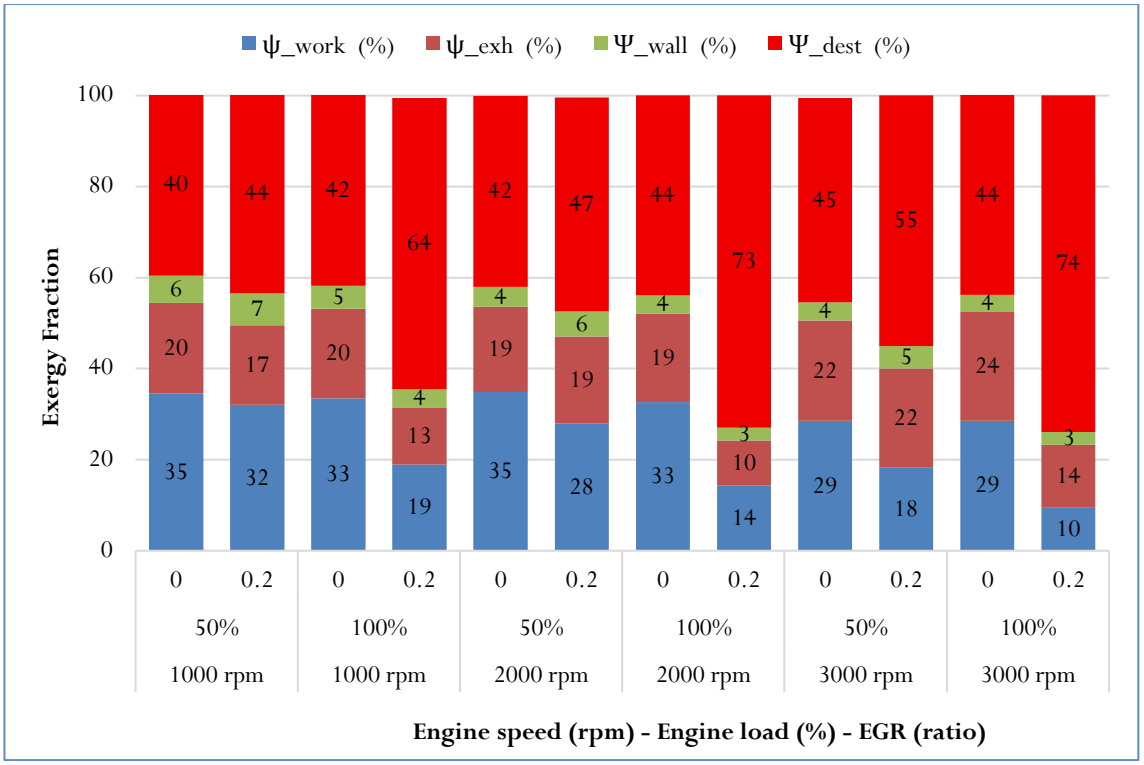

Figure 2. Speed–load distribution of exergy fractions at fixed injection timing (SOI = 9° BTDC) for EGR = 0.00 and 0.20

Figure 3 and Table A2 show the relative distribution of wall heat exergy among the cylinder head, piston, and liner at SOI = 9° BTDC for EGR levels of 0.00 and 0.20. The values are normalized to the total wall exergy at each operating point, so that each column represents 100% of the wall-related losses. Under EGR = 0.00, the piston and the cylinder head consistently carry the largest portions of the wall heat exergy. Across the examined operating points, the cylinder head contributes approximately 33–38% of the total wall heat exergy, while the piston accounts for about 34–40%, with only moderate variation as speed and load change. The liner contributes the smallest share across all conditions, typically ranging between 22% and 33%. A slight increase is observed at higher engine speeds, which may be linked to changes in heat-transfer distribution due to increased combustion intensity and elevated gas motion.

When EGR is raised to 0.20, the internal distribution shifts more gradually than the overall exergy balance shown previously. In several full-load cases, the liner fraction increases modestly (for example, at 3000 rpm and 100% load), while the shares of the head and piston decrease slightly. However, these changes are incremental rather than abrupt, indicating that EGR primarily affects the magnitude of total irreversibility rather than redistributing wall heat among individual components. This indicates that EGR modifies the combustion pathway more than the wall heat-transfer pathway at this operating condition.

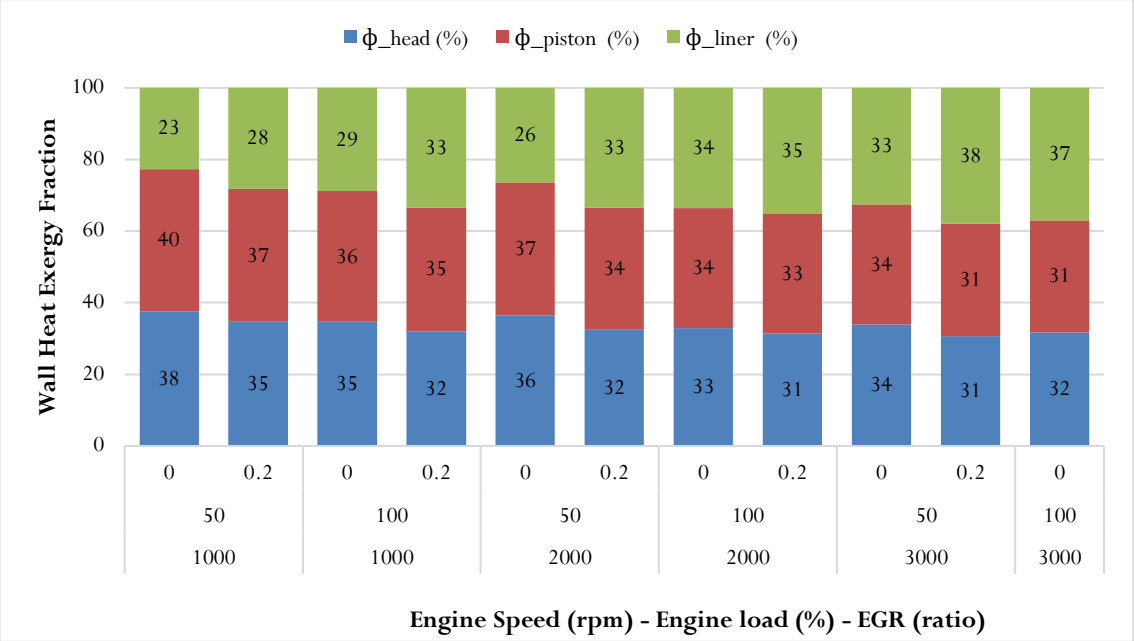

Figure 3. Component-wise distribution of wall heat exergy among the cylinder head, piston, and liner at SOI = 9° BTDC for EGR = 0.00 and 0.20

3.2 Effect of injection timing on component-wise exergy losses

Figure 4 presents the variation of component-wise wall heat exergy fractions with injection timing at 2000 rpm for 50% and 100% load conditions (EGR = 0). At 100% load, retarded injection (0° BTDC) resulted in a liner contribution of about 40%, while the cylinder head and piston accounted for roughly 29% and 30%, respectively. As injection timing is advanced toward 18° BTDC, the liner share decreases to approximately 26%, whereas the head and piston increase to nearly 37% each. Advancing injection timing brings heat release closer to top dead center. As a result, a larger portion of the flame develops while the piston crown and cylinder head are still near minimum volume, increasing local temperature gradients toward these surfaces. The piston and cylinder head were subjected to higher thermal loading, which explains their increased share of wall heat exergy.

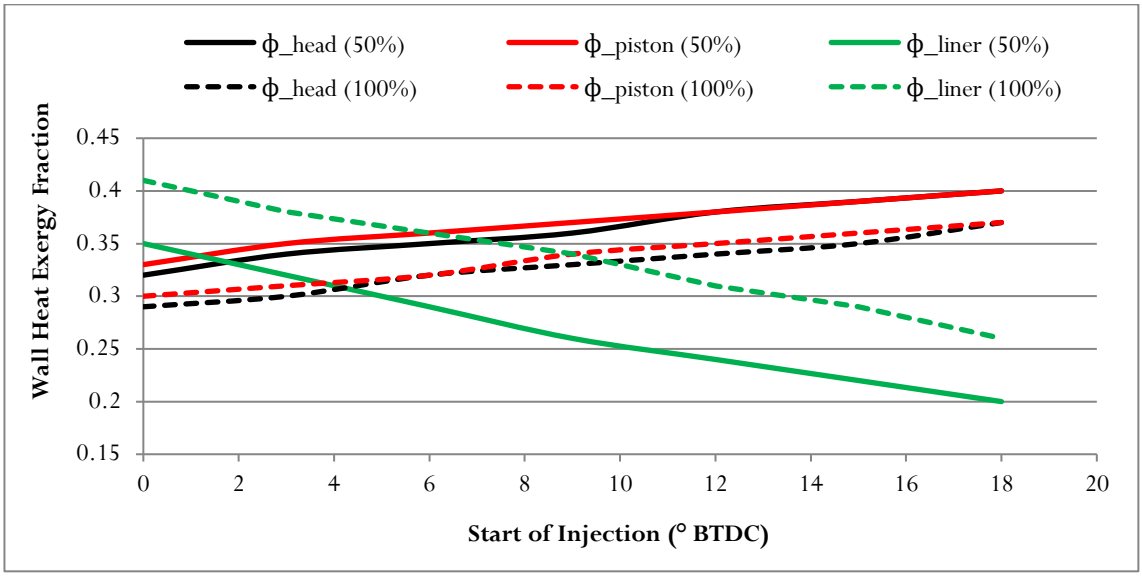

Figure 4. Component-wise wall heat exergy fractions versus injection timing at 2000 rpm for 50% and 100% load (EGR = 0)

A clearer interpretation follows from the wall–combustion interaction under advanced phasing. With earlier injection, a greater share of heat release is concentrated around top dead center, when the cylinder volume is smallest and high-temperature gases persist for a longer duration. The combustion region moves closer to the piston crown and cylinder head, which intensifies the heat flux toward these boundaries. At the same time, the shorter expansion phase restricts thermal dissipation, sustaining higher temperatures near the walls and amplifying the resulting temperature gradients. Such behavior is consistent with established combustion theory and has been reported in previous studies on diesel engines operating under advanced injection timing conditions [28], [29].

A similar but more pronounced trend is observed at 50% load. The liner fraction decreased from 35% at late injection to 20% at the most advanced setting. In parallel, the head and piston fractions increased from 32–34% to 40% each. At part load, the total heat release is lower than at full load. Injection timing directly influences the development of combustion inside the cylinder. As a result, the redistribution of wall heat exergy among the components becomes more pronounced at 50% load than at full load. At part load, combustion phasing becomes more sensitive to injection timing, so small shifts in start of injection lead to larger changes in the spatial location of heat release. These results demonstrate that injection timing governs not only the magnitude of wall heat loss, but also the spatial localization of thermal loading within the combustion chamber. Appendix (Table A2) reports the full numerical values for all SOI cases. Therefore, injection timing governs not only the magnitude of wall heat loss but also the component exposed to peak thermal loading.

3.3 Effect of EGR Rate on exergy destruction structure

Figure 5 illustrates the variation of exergy destruction (ψ_{dest}) with EGR rate at three injection timings under full-load operation. Across all timing and engine speeds, increasing the EGR rate from 0.00 to 0.20 consistently increased the destruction fraction. However, the magnitude of this increase depended strongly on the injection timing. At retarded injection (SOI = 0° BTDC), ψ_{dest} increased steadily with EGR for all speeds. For example, at 3000 rpm, ψ_{dest} increased from 0.54 at EGR = 0.00 to 0.81 at EGR = 0.20. At 2000 rpm, it increased from 0.47 to 0.78 over the same EGR range. When combustion is phased later in the cycle, introducing EGR results in a greater increase in internal irreversibility.

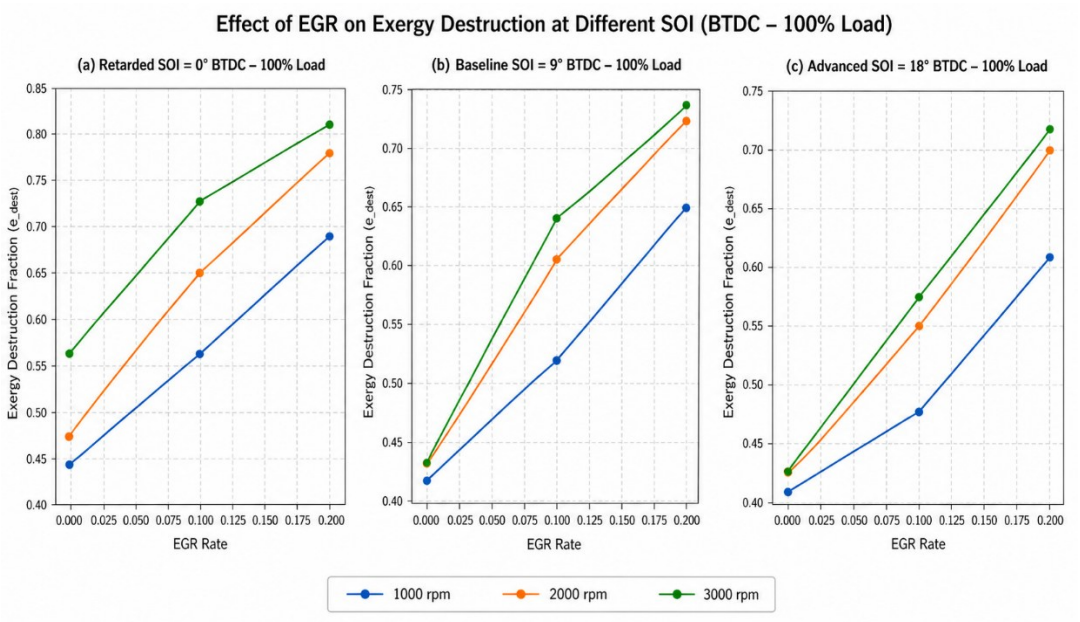

Figure 5. Influence of EGR rate on exergy destruction at different injection timings (SOI = 0°, 9°, and 18° BTDC) under full-load conditions

At the baseline timing (SOI = 9° BTDC), the same monotonic increase is evident, although the absolute levels differ slightly. At 2000 rpm, ψ_{dest} increased from 0.44 at zero EGR to 0.73 at EGR = 0.20. At 1000 rpm, the increase is more moderate, rising from 0.42 to 0.65. The detailed numerical values for all speeds and EGR settings are reported in Table A2 in the Appendix. Under advanced injection (SOI = 18° BTDC), exergy destruction remained lower at zero EGR than at retarded timing, but it still increased markedly with higher EGR rates. At 3000 rpm, ψ_{dest} increased from 0.43 to 0.72 as EGR increased to 0.20. Although advanced timing shifts combustion closer to top dead center and can improve thermodynamic conversion under low dilution, the addition of EGR offsets this benefit by increasing entropy generation.

Across the three injection timings, clear differences appeared in both the baseline level of exergy destruction and its sensitivity to EGR. At zero EGR, advanced injection (18° BTDC) yielded the lowest value of ψ_{dest}, whereas retarded injection (0° BTDC) led to the highest destruction levels, especially at higher engine speeds. For instance, at 3000 rpm and EGR = 0.00, ψ_{dest} is 0.43 for advanced timing, compared with 0.54 for retarded timing. This indicates that earlier combustion phasing improved thermodynamic conversion under undiluted conditions.

As the EGR rate increased to 0.20, the gap among the three injection timings became smaller. The trend reflects a departure from timing-governed combustion toward a dilution-dominated regime, in which the limitation in oxygen supply dictates the magnitude of thermodynamic losses. At 2000 rpm, the irreversibility level remained consistently elevated, with ψ_{dest} approaching 0.78 under delayed injection, decreasing to nearly 0.73 at the reference condition, and further to about 0.70 when injection was advanced. Under these conditions, the effect of charge dilution became more influential than the exact combustion phasing in determining the level of exergy destruction. In other words, injection timing governed the initial thermodynamic efficiency at low EGR, but as dilution increased, the combustion process became increasingly controlled by oxygen availability and mixture homogeneity. Under these conditions, the structural differences imposed by phasing are partially overshadowed by dilution-driven irreversibility.

From a physical standpoint, the rise in exergy destruction with increasing EGR can be attributed to charge dilution and reduced oxygen concentration. Reported studies indicate that EGR dilution reduces mixture reactivity and delays combustion development, leading to a longer burning period and higher entropy generation [30]. In addition, the increase in combustion duration under EGR conditions is associated with the higher specific heat capacity of the recirculated gases, which reduces the in-cylinder temperature rise and slows down reaction kinetics. Lower oxygen levels and higher thermal inertia slow and prolong the combustion process.

Accordingly, in-cylinder entropy production increases, and a larger portion of the fuel exergy is lost rather than converted into brake work. The effect becomes stronger at higher speeds, where increased fuel supply under limited oxygen conditions leads to greater losses. The results also show that the influence of EGR on exergy destruction depends on both injection timing and engine speed. At low EGR levels, advanced injection generally results in lower exergy destruction. As the EGR rate increased, however, the exergy balance shifted toward greater internal irreversibility across all injection timings. The complete quantitative trends for all operating conditions are provided in Appendix (Table A2).

3.4 Combined influence of injection timing and EGR

Figure 6 illustrates the SOI–EGR heatmaps of the total heat exergy loss from the wall at 2000 rpm under full-load and part-load (50%) conditions, while the corresponding numerical values are reported in the Appendix (Table A2). A clear load-dependent interaction between injection timing and EGR is observed.

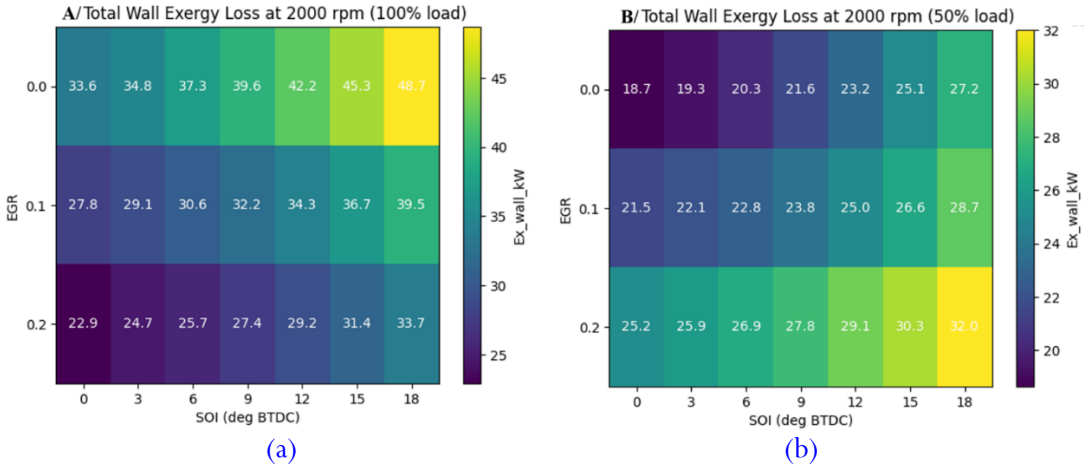

(a) (b)

Figure 6. Effect of combined injection timing and EGR on total wall heat exergy loss at 2000 rpm for full (a) and part (b) load conditions

At 100% load (Figure 6(a)), advancing the injection timing from 0° to 18° BTDC resulted in a steady increase in total wall exergy loss across all EGR levels. At zero EGR, the total wall exergy loss increased from 33.6 kW at 0° BTDC to 48.7 kW at 18° BTDC. With EGR = 0.2, the wall exergy losses are consistently lower over the entire injection timing range. The values reached 22.9 kW at 0° BTDC and 33.7 kW at 18° BTDC, compared with 33.6 kW and 48.7 kW without EGR. At advanced phasing, the reduction is close to 15 kW. This behavior is associated with the dilution of the intake charge by recirculated exhaust gases, which reduces the oxygen concentration and increases the effective heat capacity of the mixture, thereby limiting heat transfer to the chamber walls. As a result, peak combustion temperatures and temperature gradients near the chamber walls are reduced, leading to weaker convective heat transfer and, therefore, reduced wall-related exergy losses. Under high load, heat transfer is primarily governed by peak temperature gradients rather than combustion duration.

In contrast, the behavior at 50% load (Figure 6(b)) is substantially different. For EGR = 0.0, wall losses increased from 18.7 kW at 0° BTDC to 27.2 kW at 18° BTDC, following the expected trend of advanced combustion phasing. However, when EGR is introduced, the total wall exergy loss increases rather than decreases. At an EGR rate of 0.2, the wall exergy loss ranged between 25.2 kW at 0° BTDC and 32.0 kW at 18° BTDC and remained higher than the values obtained without EGR at the same injection timings.

This opposite response can be explained by the different thermodynamic regimes at the part load. Under 50% load, the baseline in-cylinder temperatures and pressures are already lower. The introduction of EGR in this regime does not primarily reduce excessively high thermal gradients, as in the full-load case. Instead, it tends to slow down combustion, extend the heat-release duration, and shift part of the combustion process deeper into the expansion stroke. The extended combustion duration increased the contact time between the high-temperature gases and the chamber walls, which raised the cumulative heat transfer. Any reduction in peak temperature is offset by this longer residence time, resulting in higher wall exergy losses. In this regime, the extended residence time of hot gases dominates the reduction in peak temperature.

The comparison between Figure 6(a) and Figure 6(b), therefore, highlights a key outcome: the combined SOI–EGR influence on wall exergy loss is strongly load-dependent. At high load, the EGR acts as a thermal moderator, reducing wall irreversibilities. Under part-load conditions, EGR dilution does not reduce wall losses; the slower, more prolonged combustion process increases the cumulative heat transfer to the chamber walls. This result, consistently reflected in Table A2, indicated that EGR cannot be evaluated independently of operating load when wall-resolved

second-law behavior is considered. The opposite responses at high and low loads reveal two competing mechanisms: temperature-driven and duration-driven heat transfer.

3.5 Speed–load sensitivity, irreversibility mapping, and trade-off behaviour

The trade-off map reveals an inverse correspondence between exergy efficiency (η_{ex}) and exergy destruction (ψ_{dest}) over the studied operating domain. As shown in Figure 7, the averaged values separate the data into four regions that reflect distinct thermodynamic regimes. Higher η_{ex} is associated with lower ψ_{dest}, indicating a more effective utilization of the fuel exergy.

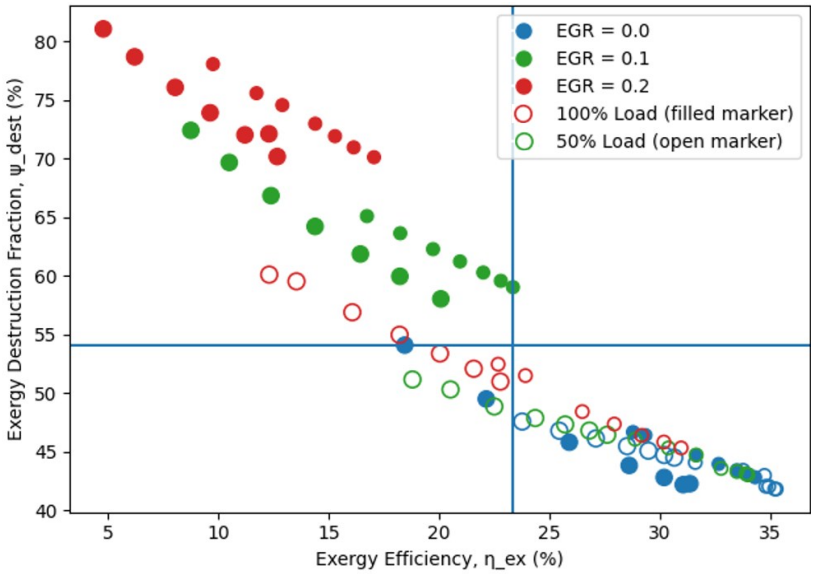

Figure 7. Trade-off relationship between $\eta_{ex}$and ψ_{dest} with EGR levels distinguished by color and load condition indicated by marker style.

In the upper-left quadrant, η_{ex} remained below 15%, whereas ψ_{dest} exceeded 70%. These points are associated with low-speed operation or retarded injection timing, where thermodynamic conversion is limited. Several cases with η_{ex} in the range of 6–10% showed ψ_{dest} above 75%, meaning that most of the supplied fuel exergy is consumed by internal irreversibilities rather than converted into brake work. The detailed numerical values for these cases are provided in the appendix (Table A2). In the central region of the map, η_{ex} lay between 18% and 22%, while ψ_{dest} ranged from 55% to 65%. Compared with the low-efficiency points, combustion occurred closer to top dead center, and the expansion process contributed more effectively to brake work. However, wall heat transfer and exhaust exergy remained considerable, and internal irreversibility still accounted for a large share of the fuel exergy.

The lower-right quadrant represented the most favorable operating region. In this region, combustion occurs close to top dead center without excessive pre-TDC heat release, allowing efficient expansion while limiting additional wall losses. Here, η_{ex} ranged between 25% and 35%, while ψ_{dest} decreased to 42–48%. These cases were mainly associated with advanced injection timing at higher load, where combustion occurred closer to top dead center. As reported in Appendix (Table A2), 3000 rpm full-load cases achieved η_{ex} values above 30% with ψ_{dest} below 45%. These outcomes indicate that a larger fraction of the supplied fuel exergy is converted into brake work, while internal irreversibilities are significantly reduced.

A separation between EGR levels is also evident in the map. Cases with EGR = 0.0 are more frequently located in the lower-right region at high load, whereas EGR = 0.2 tends to shift several

operating points toward higher ψ_{dest} values at part load. Intermediate EGR levels (0.1) generally occupy the central region of the map. This indicates that the influence of dilution on the η_{ex}–ψ_{dest} trade-off depends on both load and combustion phasing.

The trade-off behavior is associated with combustion phasing and the corresponding pressure–temperature evolution inside the cylinder. When combustion occurred late in the cycle, the effective expansion work is reduced, and a larger portion of the released energy is dissipated through entropy generation. When injection timing is advanced, the pressure rise occurs earlier in the cycle and closer to top dead center. This increased the portion of the released energy that contributed to expansion work and reduced exergy destruction. If the timing is advanced further, wall heat transfer and mechanical losses increase, and the improvement in η_{ex} becomes smaller. The grouping of points in the lower-right part of the map, therefore, reflected a narrow range of injection settings where efficiency is higher and losses remain contained.

It is important to note that ψ_{dest} represents internal irreversibility and does not include heat exergy losses from the wall directly. Nevertheless, variations in wall losses influence η_{ex} indirectly through the overall exergy balance. For the operating conditions not specifically mentioned earlier, the full set of numerical data is shown in Table A2, which confirms that η_{ex} and ψ_{dest} consistently exhibit the opposite trend across all speed and load combinations. Figure 7 indicates that the positions of operating points varies with speed and load. Full-load conditions are mainly located in the lower-right region, whereas part-load and retarded-injection cases lie in the upper-left region with higher irreversibility. The map shows the range of operation that leads to better exergy performance when using a combination of injection timing and EGR.

3.6 Practical implications and physical constraints

The trade-off map Figure 7 indicates that improved exergy performance is confined to a limited range of injection timings and operating conditions. Although several cases achieved higher η_{ex} with lower ψ_{dest}, these points were concentrated within a narrow region of advanced injection timing at high load. Outside this region, efficiency gains were either marginal or accompanied by increased wall heat losses and internal irreversibility. From a calibration standpoint, moderate advancement of injection timing at full load provided the most consistent improvement in thermodynamic performance. However, further advancement did not lead to proportional gains and, in some cases, increased thermal loading of the chamber walls. At part load, higher EGR levels shifted several operating points toward higher ψ_{dest} values, indicating that dilution alone does not guarantee improved second-law performance.

Physical operating limits must also be considered. Certain combinations of advanced injection timing and EGR resulted in physically infeasible EGR operation due to insufficient exhaust pressure relative to the Venturi throat pressure. Advancing injection timing increases early cylinder pressure and reduces blowdown pressure available to drive the EGR flow, thereby reducing the pressure difference across the Venturi. These cases define a practical boundary for feasible calibration. Therefore, the favorable region identified in Figure 7 must be interpreted within the constraints of EGR operability. Overall, the results define a restricted operating window in which exergy efficiency is improved without excessive internal irreversibility or violation of EGR system limits. Effective calibration requires simultaneous consideration of combustion phasing, wall heat transfer, and EGR feasibility rather than isolated optimization of a single parameter. Consequently, injection timing indirectly limits achievable EGR rates, defining a physically feasible operating boundary rather than a numerical limitation.

4. Conclusion

The present work evaluated how injection timing and EGR jointly influenced the distribution of exergy losses in a heavy-duty diesel engine. The analysis showed that EGR mainly increased internal irreversibility, while injection timing primarily governed the spatial distribution of wall heat losses. A small advance in injection timing improved performance at high load, but advancing it too much increased thermal loading on the chamber walls. Injection timing and EGR behaved differently depending on the operating condition. At high load, heat transfer was dominated by peak temperature effects, whereas at part load combustion duration became more influential. Consequently, favorable operation existed only within a limited region of the operating map. In addition, advanced injection reduced the pressure difference required to drive EGR flow, producing physically infeasible operating points. Therefore, injection timing not only affected efficiency but also imposed practical limits on achievable EGR rates. The results indicated that engine calibration should be based on simultaneous consideration of combustion phasing, dilution, and thermal loading. This combined exergy-based interpretation can support more reliable optimization of heavy-duty diesel engine operation. The results inform combustion control and calibration in heavy-duty diesel engines. Injection timing and EGR influence both overall efficiency and the distribution of thermal loads within the combustion chamber. Advancing injection raises the heat load on the piston crown and cylinder head, whereas high EGR levels increase internal losses associated with mixture dilution. These observations point to the need to account for component-level thermodynamic behavior when defining operating conditions. Engine settings should balance combustion phasing and dilution to limit exergy destruction without imposing excessive thermal stress on critical components. The framework presented here offers a basis for improving both efficiency and durability in diesel engine operation. Future studies may combine experimental validation with multidimensional combustion modeling to investigate spatial thermal gradients and transient exergy redistribution under realistic operating conditions.

Author's declaration

Funding statement

This research received no specific grant from funding agencies in the public, commercial, or not-for-profit sectors.

Data availability

The datasets generated and analyzed during this study are available from the author upon reasonable request, including Diesel-RK simulation outputs and processed calculation sheets supporting the reported findings.

Acknowledgements

The author acknowledges the Deanship of Scientific Research at Qassim University for its support. The author also thanks Professor Andrey Kuleshov (Moscow State Technical University) for permission to use the Diesel-RK software.

Competing interest

The author declares that there are no competing interests or conflicts of interest regarding the publication of this paper.

Ethical clearance

Not applicable

AI statement

AI-assisted language editing (QuillBot) was used solely to improve grammar and readability. The manuscript was also proofread by an English language expert to ensure linguistic accuracy and clarity. The author reviewed and verified all scientific content and takes full responsibility for the manuscript. No AI tools were used to generate research data, figures, tables, or scientific conclusions.

Publisher's and Journal's note

Universitas Negeri Padang as the publisher, and Editor of Teknomekanik state that there is no conflict of interest towards this article publication.

References

[1] J. B. Heywood, *Internal Combustion Engine Fundamentals*. McGraw-Hill, Inc, 2018.
[2] D. F. Caris and E. E. Nelson, "a new look at High Compression Engines," Jan. 1959. https://doi.org/10.4271/590015
[3] D. LIU, B. SUN, J. SONG, T. WANG, and X. MA, "Effects of thermal and pressure loads on structural deformation of liquid oxygen/methane engine combustion chamber," *Journal of Thermal Science and Technology*, vol. 15, no. 3, pp. JTST0022–JTST0022, 2020, https://doi.org/10.1299/jtst.2020jtst0022
[4] R. D. Reitz *et al.*, "IJER editorial: The future of the internal combustion engine," *International Journal of Engine Research*, vol. 21, no. 1, pp. 3–10, Jan. 2020, https://doi.org/10.1177/1468087419877990
[5] Z. Zhang *et al.*, "Effects of intake high-pressure compressed air on thermal-work conversion in a stationary diesel engine," *Int. J. Green Energy*, vol. 20, no. 3, pp. 338–351, Feb. 2023, https://doi.org/10.1080/15435075.2022.2040509
[6] W. Sun *et al.*, "Study on effects of EGR and injection strategies on the combustion and emission characteristics of ammonia/diesel dual-fuel engine," *Energy*, vol. 315, p. 134391, Jan. 2025, https://doi.org/10.1016/j.energy.2025.134391
[7] N. A. Raji, R. O. Kuku, A. O. Openibo, and E. A. Owolabi, "Influence of compression ratio on the performance characteristics of a spark ignition engine," *Journal of Production Engineering*, vol. 27, no. 1, pp. 5–12, Jun. 2024, https://doi.org/10.24867/JPE-2024-01-005
[8] G. Qiu *et al.*, "Effect of thermal conduction in cylinder wall on in-cylinder heat transfer in high-pressure liquid hydrogen pumps," *Int. J. Hydrogen Energy*, vol. 102, pp. 937–946, Feb. 2025, https://doi.org/10.1016/j.ijhydene.2025.01.086
[9] K. Shao and H. Wu, "Effect of EGR coupled fuel injection parameters on combustion and emissions," *Sci. Rep.*, vol. 16, no. 1, p. 3654, Jan. 2026, https://doi.org/10.1038/s41598-025-33858-y
[10] S. Sahoo and D. K. Srivastava, "Experimental Study of Effect of Injection Timing on Port Fuel Injection Gasoline, Port Fuel Injection Compressed Natural Gas, and Direct Injection Compressed Natural Gas Engine Performance, Combustion, and Emissions Characteristics," *J. Eng. Gas Turbine. Power*, vol. 145, no. 6, Jun. 2023, https://doi.org/10.1115/1.4056263
[11] D. Lou, G. Song, Y. Zhang, L. Fang, and Y. Deng, "Experimental study on the effects of injection pressure and injection timing on combustion and emissions in a direct-injection

hydrogen engine," *Case Studies in Thermal Engineering*, vol. 75, p. 107235, Nov. 2025, https://doi.org/10.1016/j.csite.2025.107235

[12] Z. Hu *et al.*, "High-pressure injection or low-pressure injection for a direct injection hydrogen engine?," *Int. J. Hydrogen Energy*, vol. 59, pp. 383–389, Mar. 2024, https://doi.org/10.1016/j.ijhydene.2024.02.018

[13] K. Yang *et al.*, "Impact of natural gas injection timing on the combustion and emissions performance of a dual-direct-injection diesel/natural gas engine," *Energy*, vol. 270, p. 126813, May 2023, https://doi.org/10.1016/j.energy.2023.126813

[14] H.-M. Baek, G.-S. Jung, Q. D. Vuong, J.-U. Lee, and J.-W. Lee, "Effect of Performance by Excessive Advanced Fuel Injection Timing on Marine Diesel Engine," *Applied Sciences*, vol. 13, no. 16, p. 9263, Aug. 2023, https://doi.org/10.3390/app13169263

[15] R. Chaurasiya and A. Krishnasamy, "A single fuel port and direct injected low temperature combustion strategy to reduce regulated pollutants from a light-duty diesel engine," *Fuel*, vol. 335, p. 127114, Mar. 2023, https://doi.org/10.1016/j.fuel.2022.127114

[16] J. Wasilewski *et al.*, "Evaluation of Nitrogen Oxide (NO) and Particulate Matter (PM) Emissions from Waste Biodiesel Combustion," *Energies (Basel).*, vol. 17, no. 2, p. 328, Jan. 2024, https://doi.org/10.3390/en17020328

[17] Wasiu B. Ayandotun, A. Rashid A. Aziz, And Abdullah Jamil, "Strategies for minimizing engine-out emissions in combustion engines," *International Journal of Engineering Processing and Safety Research*, Apr. 2025, https://doi.org/10.70382/caijepsr.v7i5.003

[18] B. Deng *et al.*, "A comprehensive investigation of EGR (exhaust gas recirculation) effects on energy distribution and emissions of a turbo-charging diesel engine under World Harmonized transient cycle," *Energy*, vol. 316, p. 134506, Feb. 2025, https://doi.org/10.1016/j.energy.2025.134506

[19] M. A. Ismael *et al.*, "Ammonia as a hydrogen carrier in dual-fuel diesel engines: Influence of ammonia and oxygen on combustion performance and emissions," *Int. J. Hydrogen Energy*, vol. 165, p. 150586, Sep. 2025, https://doi.org/10.1016/j.ijhydene.2025.150586

[20] Y. Lu, Y. Chen, D. Zhang, L. Zhong, Y. Qian, and Y. Pei, "Effect of pre-chamber fuel injection parameters and EGR on the combustion and emissions of a heavy-duty diesel engine," *Energy Sources, Part A: Recovery, Utilization, and Environmental Effects*, vol. 46, no. 1, pp. 6662–6684, Dec. 2024, https://doi.org/10.1080/15567036.2024.2353198

[21] K. Bayramoğlu and M. Nuran, "Energy, exergy, sustainability evaluation of the usage of pyrolytic oil and conventional fuels in diesel engines," *Process Safety and Environmental Protection*, vol. 181, pp. 324–333, Jan. 2024, https://doi.org/10.1016/j.psep.2023.11.034

[22] B. Doğan and D. Erol, "The investigation of energy and exergy analyses in compression ignition engines using diesel/biodiesel fuel blends-a review," *J. Therm. Anal. Calorim.*, vol. 148, no. 5, pp. 1765–1782, Mar. 2023, https://doi.org/10.1007/s10973-022-11862-y

[23] C. Tiwari, T. N. Verma, G. Dwivedi, and P. Verma, "Energy-Exergy Analysis of Diesel Engine Fueled with Microalgae Biodiesel-Diesel Blend," *Applied Sciences*, vol. 13, no. 3, p. 1857, Jan. 2023, https://doi.org/10.3390/app13031857

[24] J. Nie, S. Jin, J. Wang, Y. Yi, W. Su, and B. Wu, "Exergy Characteristics and Correlation Analysis of Diesel-Natural Gas Dual-Fuel Premixed Combustion," *Appl. Therm. Eng.*, vol. 278, p. 127468, Nov. 2025, https://doi.org/10.1016/j.applthermaleng.2025.127468

[25] E. F. PEHLİVAN and İ. ALTIN, "Exergy analysis under consideration of operational parameters by numerical approach in a two-stroke marine diesel engine," *Fuel*, vol. 368, p. 131650, Jul. 2024, https://doi.org/10.1016/j.fuel.2024.131650

[26] G. Kaltakkıran, H. İ. Akolaş, and K. Bakirci, "Evaluation of energy-exergy performance and sustainability index of a DI engine integrated with designed electromechanical EGR cooling system," *Energy Convers. Manag.*, vol. 290, p. 117229, Aug. 2023, https://doi.org/10.1016/j.enconman.2023.117229

[27] D. Wang, H. Zhang, Y. Qian, and K. Deng, "Experimental energy and exergy analysis of turbocharged marine low-speed engine with high pressure exhaust gas recirculation," *Fuel*, vol. 323, p. 124360, Sep. 2022, https://doi.org/10.1016/j.fuel.2022.124360

[28] J. Yan, S. Jin, W. Zhang, Z. Guo, and Y. Yuan, "Investigation of wall temperature effects on fuel spray impingement and combustion characteristics in air-cooled diesel engines during cold start," *Energy*, vol. 335, p. 138311, Oct. 2025, https://doi.org/10.1016/j.energy.2025.138311

[29] R. Y. Dahham, H. Wei, and J. Pan, "Improving Thermal Efficiency of Internal Combustion Engines: Recent Progress and Remaining Challenges," *Energies (Basel).*, vol. 15, no. 17, p. 6222, Aug. 2022, https://doi.org/10.3390/en15176222

[30] X. Yin *et al.*, "Experimental analysis of the EGR rate and temperature impact on combustion and emissions characteristics in a heavy-duty NG engine," *Fuel*, vol. 310, p. 122394, Feb. 2022, https://doi.org/10.1016/j.fuel.2021.122394

Nomenclature

Symbol	Description	Unit
$\dot{E}x_{fuel}$	Fuel exergy rate supplied to the engine	kW
$\dot{E}x_{brake}$	Brake work exergy (equal to brake power)	kW
$\dot{E}x_{exh}$	Exhaust gas physical exergy	kW
$\dot{E}x_{head}$	Exergy associated with heat transfer to surroundings	kW
$\dot{E}x_{dest}$	Exergy destruction due to irreversibilities	kW
ψ_{work}	Brake exergy fraction	–
ψ_{exh}	Exhaust exergy fraction	–
ψ_{heat}	Heat transfer exergy fraction	–
ψ_{dest}	Exergy destruction fraction	–
η_{ex}	Exergy efficiency	–
T_0	Ambient reference temperature	K
p_0	Ambient reference pressure	bar
cp	Specific heat capacity of exhaust gases	kJ/kg·K
(R	Gas constant	kJ/kg·K
LHV	Lower heating value of fuel	kJ/kg
$\dot{m}_{fuel}$	Fuel mass flow rate	kg/s
$\dot{m}_{exh}$	Exhaust gas mass flow rate	kg/s
$\dot{Q}$	Heat transfer rate	kW
T_b	Boundary (wall) temperature	K
N_{cyl}	Number of engine cylinders	–
$\dot{q}_{head}$	Heat transfer to cylinder head	W
$\dot{q}_{pist}$	Heat transfer to piston	W
$\dot{q}_{liner}$	Heat transfer to liner	W
ϕ_{head}	Head wall exergy fraction	–
ϕ_{pist}	Piston wall exergy fraction	–
ϕ_{liner}	Liner wall exergy fraction	–

APPENDIX

Table A1-a. Raw simulation results at 1000 rpm

Speed RPM	Load %	SOI °BTDC	EGR	BP kW	SFC kg/kWh	η_{BP} %	$\dot{m}_{air}$ kg/s	$\dot{m}_{fuel}$ kg/s	$\dot{m}_{exh,gas}$ kg/s	$\dot{m}_{EGR}$ kg/s	T_{exh} K	p_{exh} bar	q_{head} W	q_{pist} W	q_{liner} W	$T_{w,head}$ K	$T_{w,pist}$ K	$T_{w,liner}$ K
1000	50	0	0.0	82.9	0.2390	35.4	0.20524	0.0055	0.2052	0.0000	725	2.68	1912	1728	1896	436	480	420
1000	50	0	0.1	76.1	0.2601	32.6	0.16464	0.0055	0.1642	0.0183	819	2.35	1935	1768	2265	437	481	420
1000	50	0	0.2	72.4	0.2736	31.0	0.12684	0.0055	0.1266	0.0317	926	2.12	2095	1942	2698	443	487	420
1000	50	3	0.0	85.3	0.2322	36.5	0.20479	0.0055	0.2048	0.0000	702	2.76	2067	1874	1821	442	486	420
1000	50	3	0.1	78.4	0.2524	33.6	0.16413	0.0055	0.1628	0.0182	810	2.36	2071	1899	2235	442	486	420
1000	50	3	0.2	75.4	0.2626	32.3	0.12799	0.0055	0.1278	0.0320	897	2.18	2215	2054	2624	447	492	420
1000	50	6	0.0	86.3	0.2295	36.9	0.20348	0.0055	0.2035	0.0000	692	2.79	2240	2039	1775	448	493	420
1000	50	6	0.1	81.6	0.2426	34.9	0.16490	0.0055	0.1639	0.0183	778	2.49	2249	2064	2159	448	493	420
1000	50	6	0.2	78.1	0.2536	33.4	0.12889	0.0055	0.1288	0.0322	868	2.23	2373	2202	2549	453	498	420
1000	50	9	0.0	86.1	0.2300	36.8	0.20278	0.0055	0.2028	0.0000	681	2.84	2446	2232	1735	456	501	420
1000	50	9	0.1	82.6	0.2396	35.4	0.16483	0.0055	0.1636	0.0183	763	2.54	2437	2242	2113	455	501	420
1000	50	9	0.2	79.8	0.2483	34.1	0.12931	0.0055	0.1293	0.0323	844	2.29	2555	2374	2482	460	506	420
1000	50	12	0.0	85.3	0.2321	36.5	0.20206	0.0055	0.2021	0.0000	672	2.89	2689	2461	1698	465	511	420
1000	50	12	0.1	83.0	0.2385	35.5	0.16472	0.0055	0.1634	0.0183	750	2.58	2659	2452	2068	463	510	420
1000	50	12	0.2	80.7	0.2455	34.5	0.13010	0.0055	0.1302	0.0325	821	2.34	2761	2568	2409	467	514	420
1000	50	15	0.0	83.9	0.2361	35.9	0.20151	0.0055	0.2015	0.0000	668	2.91	2963	2720	1659	475	522	420
1000	50	15	0.1	82.4	0.2404	35.2	0.16463	0.0055	0.1634	0.0183	737	2.64	2915	2694	2022	473	520	420
1000	50	15	0.2	81.0	0.2445	34.6	0.13010	0.0055	0.1304	0.0325	804	2.40	3033	2825	2352	477	525	420
1000	50	18	0.0	81.2	0.2437	34.8	0.20088	0.0055	0.2009	0.0000	660	2.94	3269	3010	1637	486	534	420
1000	50	18	0.1	81.6	0.2426	34.9	0.16479	0.0055	0.1652	0.0183	716	2.69	3236	2996	1935	484	533	420
1000	50	18	0.2	80.1	0.2471	34.3	0.13122	0.0055	0.1316	0.0328	783	2.45	3299	3077	2281	486	535	420
1000	100	0	0.0	150.5	0.2632	32.2	0.20962	0.0110	0.2096	0.0000	1109	1.76	2602	2406	3863	461	508	420
1000	100	0	0.1	107.5	0.3683	23.0	0.14935	0.0110	0.1512	0.0166	1231	1.67	2416	2256	3924	454	500	420
1000	100	0	0.2	73.3	0.5405	15.7	0.11133	0.0110	0.1132	0.0278	1187	1.72	2174	2038	3478	446	490	420
1000	100	3	0.0	156.8	0.2525	33.5	0.20888	0.0110	0.2089	0.0000	1090	1.78	2829	2622	3841	469	516	420
1000	100	3	0.1	115.0	0.3445	24.6	0.14957	0.0110	0.1516	0.0166	1219	1.68	2601	2432	3964	461	507	420
1000	100	3	0.2	80.9	0.4896	17.3	0.11167	0.0110	0.1140	0.0279	1179	1.73	2336	2192	3539	452	497	420
1000	100	6	0.0	163.2	0.2426	34.9	0.20830	0.0110	0.2083	0.0000	1071	1.81	3123	2900	3819	480	528	420
1000	100	6	0.1	122.9	0.3222	26.3	0.15000	0.0110	0.1524	0.0167	1199	1.70	2847	2667	3981	470	517	420
1000	100	6	0.2	87.9	0.4506	18.8	0.11235	0.0110	0.1151	0.0281	1159	1.74	2531	2378	3556	459	505	420
1000	100	9	0.0	166.4	0.2380	35.6	0.20661	0.0110	0.2066	0.0000	1054	1.82	3426	3186	3768	491	540	420
1000	100	9	0.1	130.6	0.3031	27.9	0.15049	0.0110	0.1532	0.0167	1176	1.72	3168	2973	3985	482	530	420
1000	100	9	0.2	94.3	0.4199	20.2	0.11337	0.0110	0.1165	0.0283	1133	1.76	2771	2607	3541	468	514	420
1000	100	12	0.0	171.0	0.2316	36.6	0.20684	0.0110	0.2068	0.0000	1038	1.84	3837	3578	3764	506	556	420
1000	100	12	0.1	135.3	0.2926	28.9	0.15098	0.0110	0.1539	0.0168	1153	1.73	3511	3298	3948	494	543	420
1000	100	12	0.2	100.2	0.3953	21.4	0.11443	0.0110	0.1180	0.0286	1106	1.78	3080	2900	3517	479	527	420
1000	100	15	0.0	167.6	0.2364	35.8	0.20619	0.0110	0.2062	0.0000	1031	1.87	4191	3901	3681	519	573	420
1000	100	15	0.1	139.7	0.2835	29.9	0.15139	0.0110	0.1546	0.0168	1131	1.75	3940	3706	3924	510	561	420
1000	100	15	0.2	102.6	0.3861	21.9	0.11559	0.0110	0.1180	0.0289	1086	1.82	3444	3247	3459	492	541	420
1000	100	18	0.0	172.8	0.2292	37.0	0.20540	0.011	0.2054	0.0000	1002	1.89	4742	4433	3676	539	593	420
1000	100	18	0.1	140.1	0.2826	30.0	0.15139	0.011	0.1536	0.0168	1116	1.78	4411	4150	3881	527	580	420
1000	100	18	0.2	107.4	0.3687	23.0	0.11630	0.011	0.1207	0.0291	1054	1.84	3912	3693	3435	509	560	420

Table A1-b. Raw simulation results at 2000 rpm

Speed RPM	Load %	SOI °BTDC	EGR	BP kW	SFC kg/kWh	η_{BP} %	$\dot{m}_{air}$ kg/s	$\dot{m}_{fuel}$ kg/s	$\dot{m}_{exh,gas}$ kg/s	$\dot{m}_{EGR}$ kg/s	T_{exh} K	p_{exh} bar	q_{head} W	q_{pist} W	q_{liner} W	$T_{w,head}$ K	$T_{w,pist}$ K	$T_{w,liner}$ K
2000	50	0	0	157.3	0.2517	33.7	0.3597	0.0110	0.3597	0.0000	800	1.80	2670	2391	3504	463	509	420
2000	50	0	0.1	143.8	0.2754	30.8	0.2641	0.0110	0.2696	0.0293	945	1.62	2868	2620	4326	470	517	420
2000	50	0	0.2	112.9	0.3509	24.1	0.1655	0.0110	0.1704	0.0414	1201	1.45	3146	2943	5245	480	528	420
2000	50	3	0	168.1	0.2356	36.0	0.3575	0.0110	0.3575	0.0000	766	1.86	2832	2542	3304	469	516	420
2000	50	3	0.1	151.3	0.2618	32.4	0.2657	0.0110	0.2715	0.0295	919	1.65	2992	2736	4196	475	522	420
2000	50	3	0.2	119.0	0.3327	25.5	0.1689	0.0110	0.1728	0.0422	1175	1.48	3279	3068	5171	485	533	420
2000	50	6	0	173.0	0.2290	37.0	0.3567	0.0110	0.3567	0.0000	750	1.89	3019	2717	3202	475	523	420
2000	50	6	0.1	157.6	0.2514	33.7	0.2672	0.0110	0.2733	0.0297	894	1.68	3144	2877	4070	480	528	420
2000	50	6	0.2	131.9	0.3003	28.2	0.1855	0.0110	0.1907	0.0464	1114	1.59	3446	3213	5113	491	540	420
2000	50	9	0	173.9	0.2277	37.2	0.3810	0.0110	0.3810	0.0000	718	2.15	3274	2941	3072	484	533	420
2000	50	9	0.1	163.2	0.2427	34.9	0.2912	0.0110	0.2973	0.0324	838	1.89	3350	3054	3884	487	536	420
2000	50	9	0.2	139.1	0.2848	29.7	0.1902	0.0110	0.1956	0.0475	1078	1.62	3616	3369	5001	497	546	420
2000	50	12	0	175.6	0.2255	37.6	0.3802	0.0110	0.3802	0.0000	708	2.18	3529	3180	3011	494	543	420
2000	50	12	0.1	166.8	0.2375	35.7	0.2926	0.0110	0.2989	0.0325	817	1.93	3569	3258	3770	495	545	420
2000	50	12	0.2	145.3	0.2726	31.1	0.1938	0.0110	0.1996	0.0484	1047	1.64	3833	3573	4914	505	555	420
2000	50	15	0	175.3	0.2259	37.5	0.3796	0.0110	0.3796	0.0000	702	2.19	3819	3451	2957	504	555	420
2000	50	15	0.1	168.8	0.2346	36.1	0.2934	0.0110	0.3001	0.0326	800	1.96	3830	3502	3673	505	555	420
2000	50	15	0.2	150.3	0.2636	32.1	0.1990	0.0110	0.2051	0.0498	1009	1.68	4043	3767	4758	512	563	420
2000	50	18	0	173.3	0.2286	37.1	0.3787	0.0110	0.3787	0.0000	697	2.21	4131	3744	2919	515	567	420
2000	50	18	0.1	169.2	0.2340	36.2	0.2938	0.0110	0.3010	0.0327	788	1.99	4144	3797	3592	516	568	420
2000	50	18	0.2	154.2	0.2569	33.0	0.2031	0.0110	0.2098	0.0508	975	1.71	4313	4017	4618	522	574	420
2000	100	0	0	286.6	0.2764	30.7	0.3642	0.0220	0.3642	0.0000	1227	1.12	3851	3538	7335	506	556	420
2000	100	0	0.1	166.5	0.4756	17.8	0.2365	0.0220	0.2485	0.0263	1255	1.32	3299	3063	6177	486	534	420
2000	100	0	0.2	97.0	0.8162	10.4	0.1608	0.0220	0.1727	0.0402	1193	1.40	2864	2673	5008	470	517	420
2000	100	3	0	292.2	0.2711	31.3	0.3605	0.0220	0.3605	0.0000	1216	1.17	4053	3719	7192	512	565	420
2000	100	3	0.1	181.5	0.4363	19.4	0.2374	0.0220	0.2506	0.0264	1240	1.32	3482	3236	6221	492	541	420
2000	100	3	0.2	116.7	0.6789	12.5	0.1688	0.0220	0.1822	0.0422	1179	1.40	3090	2884	5206	478	526	420
2000	100	6	0	315.0	0.2514	33.7	0.3599	0.0220	0.3599	0.0000	1189	1.17	4392	4048	7227	525	577	420
2000	100	6	0.1	196.3	0.4034	21.0	0.2389	0.0220	0.2533	0.0265	1219	1.33	3701	3443	6225	500	550	420
2000	100	6	0.2	128.3	0.6172	13.7	0.1700	0.0220	0.1847	0.0425	1154	1.39	3251	3037	5175	484	532	420
2000	100	9	0	325.2	0.2435	34.8	0.3587	0.0220	0.3587	0.0000	1172	1.20	4719	4356	7146	537	590	420
2000	100	9	0.1	208.5	0.3798	22.3	0.2399	0.0220	0.2555	0.0267	1196	1.35	3945	3670	6170	509	560	420
2000	100	9	0.2	143.2	0.5532	15.3	0.1753	0.0220	0.1911	0.0438	1130	1.37	3493	3265	5202	492	542	420
2000	100	12	0	333.5	0.2375	35.7	0.3579	0.0220	0.3579	0.0000	1153	1.22	5087	4701	7056	550	605	420
2000	100	12	0.1	219.0	0.3616	23.4	0.2413	0.0220	0.2577	0.0268	1176	1.35	4242	3953	6112	519	571	420
2000	100	12	0.2	152.1	0.5208	16.3	0.1779	0.0220	0.1946	0.0445	1111	1.45	3768	3525	5189	502	552	420
2000	100	15	0	338.9	0.2337	36.2	0.3565	0.0220	0.3565	0.0000	1138	1.24	5493	5082	6974	565	622	420
2000	100	15	0.1	226.9	0.3490	24.3	0.2427	0.0220	0.2598	0.0270	1154	1.36	4585	4277	6040	532	585	420
2000	100	15	0.2	160.5	0.4934	17.2	0.1804	0.0220	0.1981	0.0451	1092	1.48	4082	3821	5147	514	565	420
2000	100	18	0	341.7	0.2318	36.5	0.3551	0.0220	0.3551	0.0000	1126	1.25	5932	5494	6902	582	640	420
2000	100	18	0.1	232.4	0.3408	24.9	0.2434	0.0220	0.2613	0.0271	1136	1.38	4969	4637	5975	546	600	420
2000	100	18	0.2	169.7	0.4667	18.1	0.1837	0.0220	0.2020	0.0459	1067	1.39	4425	4148	5085	526	578	420

Table A1-c. Raw simulation results at 3000 rpm

Speed RPM	Load %	SOI °BTDC	EGR	BP kW	SFC kg/kWh	η_{BP} %	$\dot{m}_{air}$ kg/s	$\dot{m}_{fuel}$ kg/s	$\dot{m}_{exh,gas}$ kg/s	$\dot{m}_{EGR}$ kg/s	T_{exh} K	p_{exh} bar	q_{head} W	q_{pist} W	q_{liner} W	$T_{w,head}$ K	$T_{w,pist}$ K	$T_{w,liner}$ K
3000	50	0	0	185.5	0.3348	25.3	0.5837	0.0173	0.5837	0.0000	865	1.85	3606	3176	5954	498	547	420
3000	50	0	0.1	146.7	0.4234	20.0	0.4102	0.0173	0.4161	0.0456	1073	1.63	3857	3490	7297	507	557	420
3000	50	0	0.2	96.0	0.6471	13.1	0.2972	0.0173	0.3005	0.0743	1216	1.51	4107	3782	8059	516	567	420
3000	50	3	0	198.7	0.3126	27.1	0.5838	0.0173	0.5838	0.0000	846	1.87	3717	3278	5781	502	552	420
3000	50	3	0.1	160.1	0.3878	21.8	0.4053	0.0173	0.4124	0.0450	1053	1.71	3904	3540	7080	509	559	420
3000	50	3	0.2	105.6	0.5880	14.4	0.2852	0.0173	0.2890	0.0713	1223	1.55	4078	3759	7855	515	566	420
3000	50	6	0	211.6	0.2935	28.9	0.5819	0.0173	0.5819	0.0000	825	1.90	3857	3407	5607	507	557	420
3000	50	6	0.1	175.6	0.3536	24.0	0.4140	0.0173	0.4197	0.0460	1029	1.67	4084	3700	7093	515	567	420
3000	50	6	0.2	125.4	0.4953	17.1	0.2892	0.0173	0.2936	0.0723	1210	1.54	4244	3914	7920	521	573	420
3000	50	9	0	222.6	0.2789	30.4	0.5842	0.0173	0.5842	0.0000	805	1.94	4027	3561	5433	513	564	420
3000	50	9	0.1	190.1	0.3267	25.9	0.4165	0.0173	0.4238	0.0463	1000	1.70	4212	3815	6884	520	572	420
3000	50	9	0.2	142.1	0.4370	19.4	0.2893	0.0173	0.2945	0.0723	1195	1.56	4404	4064	7892	527	579	420
3000	50	12	0	230.2	0.2698	31.4	0.5792	0.0173	0.5792	0.0000	794	1.96	4218	3740	5310	520	572	420
3000	50	12	0.1	200.7	0.3094	27.4	0.4186	0.0173	0.4263	0.0465	973	1.72	4368	3957	6705	525	578	420
3000	50	12	0.2	156.4	0.3970	21.3	0.2919	0.0173	0.2976	0.0730	1175	1.57	4579	4227	7842	533	586	420
3000	50	15	0	235.7	0.2634	32.2	0.5774	0.0173	0.5774	0.0000	783	1.98	4437	3943	5198	528	581	420
3000	50	15	0.1	209.3	0.2967	28.5	0.4202	0.0173	0.4282	0.0467	953	1.74	4554	4130	6550	532	585	420
3000	50	15	0.2	168.4	0.3689	23.0	0.2944	0.0173	0.3006	0.0736	1156	1.57	4777	4412	7785	540	594	420
3000	50	18	0	239.3	0.2595	32.6	0.5759	0.0173	0.5759	0.0000	774	2.00	4696	4183	5102	537	591	420
3000	50	18	0.1	215.6	0.2881	29.4	0.4216	0.0173	0.4297	0.0468	935	1.76	4762	4322	6410	540	594	420
3000	50	18	0.2	177.8	0.3493	24.3	0.2955	0.0173	0.3019	0.0739	1142	1.59	4997	4616	7687	548	603	420
3000	100	0	0	287.9	0.4315	19.6	0.6445	0.0345	0.6445	0.0000	1211	1.57	4788	4283	1068	541	595	420
3000	100	0	0.1	136.5	0.9099	09.3	0.4336	0.0345	0.4416	0.0482	1191	1.62	4159	3770	8600	518	570	420
3000	100	0	0.2	74.5	1.6673	05.1	0.3454	0.0345	0.3518	0.0864	1126	1.66	3972	3614	7652	511	562	420
3000	100	3	0	345.6	0.3594	23.6	0.6441	0.0345	0.6441	0.0000	1231	1.55	5186	4655	11270	556	611	420
3000	100	3	0.1	163.7	0.7588	11.2	0.4285	0.0345	0.4378	0.0476	1234	1.59	4412	4014	9148	527	580	420
3000	100	3	0.2	96.7	1.2843	06.6	0.3389	0.0345	0.3464	0.0847	1181	1.63	4223	3860	8270	520	572	420
3000	100	6	0	404.4	0.3072	27.6	0.6425	0.0345	0.6425	0.0000	1224	1.55	5621	5060	11559	572	629	420
3000	100	6	0.1	193.2	0.6429	13.2	0.4237	0.0345	0.4343	0.0471	1273	1.57	4698	4288	9653	537	591	420
3000	100	6	0.2	125.4	0.9903	08.6	0.3392	0.0345	0.3478	0.0848	1219	1.47	4482	4107	8844	529	582	420
3000	100	9	0	446.7	0.2780	30.5	0.6449	0.0345	0.6449	0.0000	1193	1.57	6018	5424	11471	587	646	420
3000	100	9	0.1	224.4	0.5535	15.3	0.4236	0.0345	0.4355	0.0471	1290	1.55	5006	4582	10042	549	603	420
3000	100	9	0.2	150.1	0.8273	10.2	0.3387	0.0345	0.3483	0.0847	1242	1.45	4734	4347	9193	539	593	420
3000	100	12	0	471.5	0.2634	32.2	0.6396	0.0345	0.6396	0.0000	1176	1.58	6410	5787	11398	602	662	420
3000	100	12	0.1	256.5	0.4843	17.5	0.4206	0.0345	0.4345	0.0467	1297	1.54	5346	4901	10293	562	618	420
3000	100	12	0.2	174.8	0.7107	11.9	0.3380	0.0345	0.3490	0.0845	1246	1.48	5010	4606	9384	549	604	420
3000	100	15	0	489.7	0.2536	33.4	0.6377	0.0345	0.6377	0.0000	1152	1.59	6812	6157	11186	617	678	420
3000	100	15	0.1	284.4	0.4367	19.4	0.4206	0.0345	0.4363	0.0467	1290	1.55	5697	5229	10420	575	632	420
3000	100	15	0.2	197.6	0.6285	13.5	0.3349	0.0345	0.3479	0.0837	1250	1.64	5341	4922	9537	561	617	420
3000	100	18	0	485.0	0.2561	33.1	0.6364	0.0345	0.6364	0.0000	1158	1.61	7214	6528	11038	632	695	420
3000	100	18	0.1	313.4	0.3963	21.4	0.4213	0.0345	0.4399	0.0468	1276	1.55	6137	5639	10471	591	651	420
3000	100	18	0.2	191.7	0.6478	13.1	0.3154	0.0345	0.3288	0.0789	1226	1.42	5235	4832	8943	557	613	420

Table A2-a. Calculated terms for all simulated cases at 1000 rpm

Case ID	$\dot{E}x_{fuel}$ kW	$\dot{E}x_{brake}$ kW	η_{ex}	$\dot{E}x_{exh}$ kW	$\dot{E}x_{head}$ kW	$\dot{E}x_{pist}$ kW	$\dot{E}x_{liner}$ kW	$\dot{E}x_{wall}$ kW	ϕ_{head}	ϕ_{piston}	ϕ_{liner}	$\dot{E}x_{dest}$ kW	ψ_{brake}	ψ_{exh}	ψ_{wall}	ψ_{dest}
1000_50%_0BTDC_EGR=0	248.94	82.86	0.333	54.877	3.840	4.098	3.521	11.458	0.335	0.358	0.307	99.74	0.333	0.220	0.046	0.401
1000_50%_0BTDC_EGR=0.1	248.94	76.12	0.306	52.718	3.902	4.207	4.207	12.316	0.317	0.342	0.342	107.79	0.306	0.212	0.049	0.433
1000_50%_0BTDC_EGR=0.2	248.94	72.38	0.291	49.455	4.338	4.714	5.010	14.062	0.308	0.335	0.356	113.04	0.291	0.199	0.056	0.454
1000_50%_3BTDC_EGR=0	248.94	85.26	0.342	52.138	4.265	4.536	3.382	12.183	0.350	0.372	0.278	99.36	0.342	0.209	0.049	0.399
1000_50%_3BTDC_EGR=0.1	248.94	78.44	0.315	51.262	4.273	4.593	4.150	13.016	0.328	0.353	0.319	106.22	0.315	0.206	0.052	0.427
1000_50%_3BTDC_EGR=0.2	248.94	75.40	0.303	47.395	4.675	5.061	4.874	14.610	0.320	0.346	0.334	111.54	0.303	0.190	0.059	0.448
1000_50%_6BTDC_EGR=0	248.94	86.28	0.347	50.617	4.747	5.034	3.297	13.079	0.363	0.385	0.252	98.96	0.347	0.203	0.053	0.398
1000_50%_6BTDC_EGR=0.1	248.94	81.61	0.328	48.629	4.769	5.105	4.010	13.884	0.343	0.368	0.289	104.82	0.328	0.195	0.056	0.421
1000_50%_6BTDC_EGR=0.2	248.94	78.08	0.314	45.302	5.123	5.524	4.733	15.380	0.333	0.359	0.308	110.18	0.314	0.182	0.062	0.443
1000_50%_9BTDC_EGR=0	248.94	86.10	0.346	49.421	5.340	5.645	3.222	14.208	0.376	0.397	0.227	99.21	0.346	0.199	0.057	0.399
1000_50%_9BTDC_EGR=0.1	248.94	82.64	0.332	47.180	5.311	5.664	3.924	14.898	0.356	0.380	0.263	104.22	0.332	0.190	0.060	0.419
1000_50%_9BTDC_EGR=0.2	248.94	79.76	0.320	43.541	5.659	6.075	4.610	16.344	0.346	0.372	0.282	109.30	0.320	0.175	0.066	0.439
1000_50%_12BTDC_EGR=0	248.94	85.32	0.343	48.406	6.065	6.387	3.153	15.605	0.389	0.409	0.202	99.61	0.343	0.194	0.063	0.400
1000_50%_12BTDC_EGR=0.1	248.94	83.02	0.333	45.824	5.970	6.341	3.840	16.151	0.370	0.393	0.238	103.95	0.333	0.184	0.065	0.418
1000_50%_12BTDC_EGR=0.2	248.94	80.67	0.324	41.942	6.283	6.713	4.474	17.471	0.360	0.384	0.256	108.86	0.324	0.168	0.070	0.437
1000_50%_15BTDC_EGR=0	248.94	83.85	0.337	47.779	6.916	7.256	3.082	17.253	0.401	0.421	0.179	100.06	0.337	0.192	0.069	0.402
1000_50%_15BTDC_EGR=0.1	248.94	82.37	0.331	44.754	6.759	7.148	3.756	17.663	0.383	0.405	0.213	104.16	0.331	0.180	0.071	0.418
1000_50%_15BTDC_EGR=0.2	248.94	80.98	0.325	40.638	7.134	7.584	4.368	19.086	0.374	0.397	0.229	108.24	0.325	0.163	0.077	0.435
1000_50%_18BTDC_EGR=0	248.94	81.23	0.326	46.870	7.902	8.255	3.039	19.196	0.412	0.430	0.158	101.64	0.326	0.188	0.077	0.408
1000_50%_18BTDC_EGR=0.1	248.94	81.62	0.328	43.178	7.789	8.191	3.593	19.574	0.398	0.418	0.184	104.57	0.328	0.173	0.079	0.420
1000_50%_18BTDC_EGR=0.2	248.94	80.12	0.322	39.288	7.991	8.454	4.236	20.680	0.386	0.409	0.205	108.85	0.322	0.158	0.083	0.437
1000_100%_0BTDC_EGR=0	497.88	150.46	0.302	108.810	5.801	6.189	7.174	19.164	0.303	0.323	0.374	219.45	0.302	0.219	0.038	0.441
1000_100%_0BTDC_EGR=0.1	497.88	107.51	0.216	93.045	5.244	5.683	7.287	18.214	0.288	0.312	0.400	279.11	0.216	0.187	0.037	0.561
1000_100%_0BTDC_EGR=0.2	497.88	73.27	0.147	65.810	4.561	4.998	6.458	16.017	0.285	0.312	0.403	342.78	0.147	0.132	0.032	0.688
1000_100%_3BTDC_EGR=0	497.88	156.82	0.315	105.438	6.489	6.896	7.134	20.519	0.316	0.336	0.348	215.10	0.315	0.212	0.041	0.432
1000_100%_3BTDC_EGR=0.1	497.88	114.95	0.231	91.863	5.788	6.248	7.361	19.397	0.298	0.322	0.379	271.67	0.231	0.185	0.039	0.546
1000_100%_3BTDC_EGR=0.2	497.88	80.88	0.162	65.552	5.018	5.477	6.573	17.068	0.294	0.321	0.385	334.38	0.162	0.132	0.034	0.672
1000_100%_6BTDC_EGR=0	497.88	163.22	0.328	102.228	7.420	7.846	7.092	22.357	0.332	0.351	0.317	210.08	0.328	0.205	0.045	0.422
1000_100%_6BTDC_EGR=0.1	497.88	122.89	0.247	89.878	6.545	7.028	7.393	20.966	0.312	0.335	0.353	264.15	0.247	0.181	0.042	0.531
1000_100%_6BTDC_EGR=0.2	497.88	87.89	0.177	64.333	5.589	6.072	6.603	18.264	0.306	0.332	0.362	327.40	0.177	0.129	0.037	0.658
1000_100%_9BTDC_EGR=0	497.88	166.41	0.334	98.589	8.416	8.855	6.997	24.269	0.347	0.365	0.288	208.61	0.334	0.198	0.049	0.419
1000_100%_9BTDC_EGR=0.1	497.88	130.64	0.262	87.586	7.567	8.075	7.401	23.043	0.328	0.350	0.321	256.61	0.262	0.176	0.046	0.515
1000_100%_9BTDC_EGR=0.2	497.88	94.31	0.189	62.735	6.314	6.821	6.575	19.710	0.320	0.346	0.334	321.13	0.189	0.126	0.040	0.645
1000_100%_12BTDC_EGR=0	497.88	171.00	0.343	96.370	9.828	10.277	6.990	27.095	0.363	0.379	0.258	203.42	0.343	0.194	0.054	0.409
1000_100%_12BTDC_EGR=0.1	497.88	135.33	0.272	85.138	8.696	9.225	7.333	25.254	0.344	0.365	0.290	252.16	0.272	0.171	0.051	0.506
1000_100%_12BTDC_EGR=0.2	497.88	100.17	0.201	61.096	7.283	7.816	6.531	21.630	0.337	0.361	0.302	314.99	0.201	0.123	0.043	0.633
1000_100%_15BTDC_EGR=0	497.88	167.55	0.337	95.140	11.089	11.551	6.837	29.476	0.376	0.392	0.232	205.72	0.337	0.191	0.059	0.413
1000_100%_15BTDC_EGR=0.1	497.88	139.70	0.281	82.900	10.187	10.733	7.288	28.207	0.361	0.380	0.258	247.07	0.281	0.167	0.057	0.496
1000_100%_15BTDC_EGR=0.2	497.88	102.56	0.206	59.330	8.478	9.039	6.424	23.941	0.354	0.378	0.268	312.05	0.206	0.119	0.048	0.627
1000_100%_18BTDC_EGR=0	497.88	172.81	0.347	90.251	13.146	13.588	6.827	33.561	0.392	0.405	0.203	201.26	0.347	0.181	0.067	0.404
1000_100%_18BTDC_EGR=0.1	497.88	140.13	0.281	80.739	11.897	12.457	7.208	31.561	0.377	0.395	0.228	245.45	0.281	0.162	0.063	0.493
1000_100%_18BTDC_EGR=0.2	497.88	107.40	0.216	57.734	10.093	10.674	6.380	27.146	0.372	0.393	0.235	305.60	0.216	0.116	0.055	0.614

Table A2-b. Calculated terms for all simulated cases at 2000 rpm

Case ID	$\dot{E}x_{fuel}$ kW	$\dot{E}x_{brake}$ kW	η_{ex}	$\dot{E}x_{exh}$ kW	$\dot{E}x_{head}$ kW	$\dot{E}x_{pist}$ kW	$\dot{E}x_{liner}$ kW	$\dot{E}x_{wall}$ kW	ϕ_{head}	ϕ_{piston}	ϕ_{liner}	$\dot{E}x_{dest}$ kW	ψ_{brake}	ψ_{exh}	ψ_{wall}	ψ_{dest}
2000_50%_0BTDC_EGR=0	497.88	157.34	0.316	102.457	5.978	6.171	6.507	18.656	0.320	0.331	0.349	219.43	0.316	0.206	0.037	0.441
2000_50%_0BTDC_EGR=0.1	497.88	143.77	0.289	103.249	6.593	6.906	8.034	21.533	0.306	0.321	0.373	229.33	0.289	0.207	0.043	0.461
2000_50%_0BTDC_EGR=0.2	497.88	112.86	0.227	98.638	7.475	7.964	9.741	25.180	0.297	0.316	0.387	261.20	0.227	0.198	0.051	0.525
2000_50%_3BTDC_EGR=0	497.88	168.12	0.338	94.332	6.485	6.677	6.136	19.298	0.336	0.346	0.318	216.13	0.338	0.189	0.039	0.434
2000_50%_3BTDC_EGR=0.1	497.88	151.29	0.304	98.906	6.983	7.297	7.793	22.072	0.316	0.331	0.353	225.61	0.304	0.199	0.044	0.453
2000_50%_3BTDC_EGR=0.2	497.88	119.02	0.239	96.585	7.908	8.399	9.603	25.910	0.305	0.324	0.371	256.37	0.239	0.194	0.052	0.515
2000_50%_6BTDC_EGR=0	497.88	172.96	0.347	90.700	7.063	7.261	5.947	20.271	0.348	0.358	0.293	213.95	0.347	0.182	0.041	0.430
2000_50%_6BTDC_EGR=0.1	497.88	157.55	0.316	94.925	7.463	7.779	7.558	22.800	0.327	0.341	0.331	222.61	0.316	0.191	0.046	0.447
2000_50%_6BTDC_EGR=0.2	497.88	131.85	0.265	98.107	8.458	8.920	9.495	26.873	0.315	0.332	0.353	241.05	0.265	0.197	0.054	0.484
2000_50%_9BTDC_EGR=0	497.88	173.94	0.349	93.008	7.886	8.043	5.706	21.635	0.365	0.372	0.264	209.30	0.349	0.187	0.043	0.420
2000_50%_9BTDC_EGR=0.1	497.88	163.17	0.328	94.043	8.138	8.410	7.213	23.760	0.342	0.354	0.304	216.91	0.328	0.189	0.048	0.436
2000_50%_9BTDC_EGR=0.2	497.88	139.07	0.279	95.236	9.029	9.486	9.288	27.803	0.325	0.341	0.334	235.77	0.279	0.191	0.056	0.474
2000_50%_12BTDC_EGR=0	497.88	175.62	0.353	90.892	8.736	8.889	5.592	23.217	0.376	0.383	0.241	208.15	0.353	0.183	0.047	0.418
2000_50%_12BTDC_EGR=0.1	497.88	166.75	0.335	90.529	8.874	9.142	7.002	25.018	0.355	0.365	0.280	215.58	0.335	0.182	0.050	0.433
2000_50%_12BTDC_EGR=0.2	497.88	145.27	0.292	92.512	9.784	10.236	9.127	29.146	0.336	0.351	0.313	230.95	0.292	0.186	0.059	0.464
2000_50%_15BTDC_EGR=0	497.88	175.27	0.352	89.342	9.733	9.878	5.491	25.103	0.388	0.394	0.219	208.17	0.352	0.179	0.050	0.418
2000_50%_15BTDC_EGR=0.1	497.88	168.79	0.339	87.818	9.777	10.039	6.822	26.638	0.367	0.377	0.256	214.64	0.339	0.176	0.054	0.431
2000_50%_15BTDC_EGR=0.2	497.88	150.25	0.302	89.165	10.527	10.967	8.836	30.330	0.347	0.362	0.291	228.14	0.302	0.179	0.061	0.458
2000_50%_18BTDC_EGR=0	497.88	173.27	0.348	88.049	10.838	10.971	5.421	27.230	0.398	0.403	0.199	209.33	0.348	0.177	0.055	0.420
2000_50%_18BTDC_EGR=0.1	497.88	169.20	0.340	85.803	10.888	11.141	6.671	28.700	0.379	0.388	0.232	214.18	0.340	0.172	0.058	0.430
2000_50%_18BTDC_EGR=0.2	497.88	154.16	0.310	86.102	11.497	11.926	8.576	32.000	0.359	0.373	0.268	225.62	0.310	0.173	0.064	0.453
2000_100%_0BTDC_EGR=0	995.76	286.59	0.288	210.798	9.852	10.157	13.621	33.631	0.293	0.302	0.405	464.75	0.288	0.212	0.034	0.467
2000_100%_0BTDC_EGR=0.1	995.76	166.52	0.167	153.104	7.975	8.401	11.472	27.849	0.286	0.302	0.412	648.29	0.167	0.154	0.028	0.651
2000_100%_0BTDC_EGR=0.2	995.76	97.04	0.097	98.287	6.578	7.041	9.301	22.920	0.287	0.307	0.406	777.52	0.097	0.099	0.023	0.781
2000_100%_3BTDC_EGR=0	995.76	292.20	0.293	206.679	10.555	10.870	13.357	34.781	0.303	0.313	0.384	462.10	0.293	0.208	0.035	0.464
2000_100%_3BTDC_EGR=0.1	995.76	181.54	0.182	151.359	8.577	9.013	11.554	29.144	0.294	0.309	0.396	633.72	0.182	0.152	0.029	0.636
2000_100%_3BTDC_EGR=0.2	995.76	116.66	0.117	101.565	7.296	7.765	9.668	24.729	0.295	0.314	0.391	752.81	0.117	0.102	0.025	0.756
2000_100%_6BTDC_EGR=0	995.76	315.04	0.316	198.277	11.790	12.088	13.422	37.299	0.316	0.324	0.360	445.15	0.316	0.199	0.037	0.447
2000_100%_6BTDC_EGR=0.1	995.76	196.34	0.197	148.560	9.322	9.763	11.560	30.645	0.304	0.319	0.377	620.22	0.197	0.149	0.031	0.623
2000_100%_6BTDC_EGR=0.2	995.76	128.31	0.129	99.058	7.819	8.296	9.611	25.726	0.304	0.322	0.374	742.67	0.129	0.099	0.026	0.746
2000_100%_9BTDC_EGR=0	995.76	325.23	0.327	193.342	13.009	13.293	13.271	39.573	0.329	0.336	0.335	437.62	0.327	0.194	0.040	0.439
2000_100%_9BTDC_EGR=0.1	995.76	208.51	0.209	145.252	10.172	10.617	11.459	32.248	0.315	0.329	0.355	609.75	0.209	0.146	0.032	0.612
2000_100%_9BTDC_EGR=0.2	995.76	143.17	0.144	98.378	8.615	9.098	9.660	27.373	0.315	0.332	0.353	726.84	0.144	0.099	0.027	0.730
2000_100%_12BTDC_EGR=0	995.76	333.47	0.335	187.731	14.429	14.687	13.103	42.219	0.342	0.348	0.310	432.34	0.335	0.189	0.042	0.434
2000_100%_12BTDC_EGR=0.1	995.76	219.00	0.220	142.160	11.242	11.680	11.350	34.272	0.328	0.341	0.331	600.33	0.220	0.143	0.034	0.603
2000_100%_12BTDC_EGR=0.2	995.76	152.09	0.153	98.181	9.556	10.042	9.637	29.235	0.327	0.344	0.330	716.26	0.153	0.099	0.029	0.719
2000_100%_15BTDC_EGR=0	995.76	338.93	0.340	183.218	16.044	16.267	12.951	45.262	0.354	0.359	0.286	428.35	0.340	0.184	0.045	0.430
2000_100%_15BTDC_EGR=0.1	995.76	226.94	0.228	138.893	12.505	12.936	11.217	36.658	0.341	0.353	0.306	593.27	0.228	0.139	0.037	0.596
2000_100%_15BTDC_EGR=0.2	995.76	160.53	0.161	97.145	10.661	11.148	9.559	31.368	0.340	0.355	0.305	706.72	0.161	0.098	0.032	0.710
2000_100%_18BTDC_EGR=0	995.76	341.71	0.343	179.084	17.845	18.022	12.819	48.685	0.367	0.370	0.263	426.28	0.343	0.180	0.049	0.428
2000_100%_18BTDC_EGR=0.1	995.76	232.40	0.233	135.998	13.972	14.386	11.097	39.454	0.354	0.365	0.281	587.91	0.233	0.137	0.040	0.590
2000_100%_18BTDC_EGR=0.2	995.76	169.69	0.170	93.945	11.912	12.394	9.443	33.748	0.353	0.367	0.280	698.38	0.170	0.094	0.034	0.701

Table A2-c. Calculated terms for all simulated cases at 3000 rpm

Case ID	$\dot{E}x_{fuel}$ kW	$\dot{E}x_{brake}$ kW	η_{ex}	$\dot{E}x_{exh}$ kW	$\dot{E}x_{head}$ kW	$\dot{E}x_{pist}$ kW	$\dot{E}x_{liner}$ kW	$\dot{E}x_{wall}$ kW	ϕ_{head}	ϕ_{piston}	ϕ_{liner}	$\dot{E}x_{dest}$ kW	ψ_{brake}	ψ_{exh}	ψ_{wall}	ψ_{dest}
3000_50%_0BTDC_EGR=0	780.77	185.51	0.238	194.822	9.025	8.959	11.057	29.041	0.311	0.308	0.381	371.40	0.238	0.250	0.037	0.476
3000_50%_0BTDC_EGR=0.1	780.77	146.67	0.188	201.167	9.892	10.042	13.552	33.485	0.295	0.300	0.405	399.45	0.188	0.258	0.043	0.512
3000_50%_0BTDC_EGR=0.2	780.77	95.97	0.123	178.637	10.781	11.085	14.967	36.833	0.293	0.301	0.406	469.33	0.123	0.229	0.047	0.601
3000_50%_3BTDC_EGR=0	780.77	198.65	0.254	187.366	9.409	9.330	10.736	29.475	0.319	0.317	0.364	365.28	0.254	0.240	0.038	0.468
3000_50%_3BTDC_EGR=0.1	780.77	160.13	0.205	194.448	10.068	10.215	13.148	33.431	0.301	0.306	0.393	392.76	0.205	0.249	0.043	0.503
3000_50%_3BTDC_EGR=0.2	780.77	105.62	0.135	174.024	10.681	11.002	14.588	36.270	0.294	0.303	0.402	464.86	0.135	0.223	0.046	0.595
3000_50%_6BTDC_EGR=0	780.77	211.56	0.271	178.956	9.898	9.806	10.412	30.116	0.329	0.326	0.346	360.14	0.271	0.229	0.039	0.461
3000_50%_6BTDC_EGR=0.1	780.77	175.63	0.225	188.973	10.708	10.835	13.173	34.715	0.308	0.312	0.379	381.45	0.225	0.242	0.044	0.489
3000_50%_6BTDC_EGR=0.2	780.77	125.38	0.161	173.547	11.288	11.598	14.709	37.595	0.300	0.309	0.391	444.25	0.161	0.222	0.048	0.569
3000_50%_9BTDC_EGR=0	780.77	222.63	0.285	172.155	10.501	10.384	10.089	30.974	0.339	0.335	0.326	355.01	0.285	0.220	0.040	0.455
3000_50%_9BTDC_EGR=0.1	780.77	190.11	0.243	181.689	11.170	11.279	12.785	35.234	0.317	0.320	0.363	373.74	0.243	0.233	0.045	0.479
3000_50%_9BTDC_EGR=0.2	780.77	142.12	0.182	170.724	11.873	12.178	14.656	38.706	0.307	0.315	0.379	429.22	0.182	0.219	0.050	0.550
3000_50%_12BTDC_EGR=0	780.77	230.16	0.295	166.526	11.192	11.061	9.861	32.114	0.349	0.344	0.307	351.97	0.295	0.213	0.041	0.451
3000_50%_12BTDC_EGR=0.1	780.77	200.69	0.257	174.607	11.739	11.829	12.453	36.020	0.326	0.328	0.346	369.45	0.257	0.224	0.046	0.473
3000_50%_12BTDC_EGR=0.2	780.77	156.41	0.200	167.693	12.526	12.818	14.564	39.907	0.314	0.321	0.365	416.76	0.200	0.215	0.051	0.534
3000_50%_15BTDC_EGR=0	780.77	235.74	0.302	162.421	11.999	11.843	9.654	33.496	0.358	0.354	0.288	349.11	0.302	0.208	0.043	0.447
3000_50%_15BTDC_EGR=0.1	780.77	209.28	0.268	169.007	12.431	12.500	12.163	37.094	0.335	0.337	0.328	365.39	0.268	0.216	0.048	0.468
3000_50%_15BTDC_EGR=0.2	780.77	168.35	0.216	164.528	13.277	13.552	14.457	41.287	0.322	0.328	0.350	406.60	0.216	0.211	0.053	0.521
3000_50%_18BTDC_EGR=0	780.77	239.31	0.307	158.863	12.967	12.782	9.475	35.224	0.368	0.363	0.269	347.37	0.307	0.203	0.045	0.445
3000_50%_18BTDC_EGR=0.1	780.77	215.57	0.276	164.221	13.220	13.264	11.904	38.388	0.344	0.346	0.310	362.59	0.276	0.210	0.049	0.464
3000_50%_18BTDC_EGR=0.2	780.77	177.78	0.228	162.169	14.128	14.385	14.275	42.788	0.330	0.336	0.334	398.03	0.228	0.208	0.055	0.510
3000_100%_0BTDC_EGR=0	1561.54	287.87	0.184	382.665	13.321	13.169	19.832	46.322	0.288	0.284	0.428	844.68	0.184	0.245	0.030	0.541
3000_100%_0BTDC_EGR=0.1	1561.54	136.49	0.087	256.091	10.977	11.101	15.972	38.050	0.288	0.292	0.420	1130.91	0.087	0.164	0.024	0.724
3000_100%_0BTDC_EGR=0.2	1561.54	74.49	0.048	185.851	10.300	10.493	14.210	35.002	0.294	0.300	0.406	1266.20	0.048	0.119	0.022	0.811
3000_100%_3BTDC_EGR=0	1561.54	345.56	0.221	392.550	14.874	14.678	20.930	50.482	0.295	0.291	0.415	772.95	0.221	0.251	0.032	0.495
3000_100%_3BTDC_EGR=0.1	1561.54	163.67	0.105	268.808	11.901	12.033	16.990	40.924	0.291	0.294	0.415	1088.14	0.105	0.172	0.026	0.697
3000_100%_3BTDC_EGR=0.2	1561.54	96.71	0.062	197.904	11.203	11.416	15.359	37.978	0.295	0.301	0.404	1228.95	0.062	0.127	0.024	0.787
3000_100%_6BTDC_EGR=0	1561.54	404.35	0.259	387.499	16.628	16.369	21.467	54.464	0.305	0.301	0.394	715.23	0.259	0.248	0.035	0.458
3000_100%_6BTDC_EGR=0.1	1561.54	193.19	0.124	280.437	12.975	13.106	17.927	44.008	0.295	0.298	0.407	1043.90	0.124	0.180	0.028	0.669
3000_100%_6BTDC_EGR=0.2	1561.54	125.42	0.080	206.939	12.158	12.373	16.425	40.956	0.297	0.302	0.401	1188.22	0.080	0.133	0.026	0.761
3000_100%_9BTDC_EGR=0	1561.54	446.72	0.286	373.041	18.270	17.926	21.303	57.500	0.318	0.312	0.370	684.28	0.286	0.239	0.037	0.438
3000_100%_9BTDC_EGR=0.1	1561.54	224.40	0.144	287.165	14.163	14.277	18.649	47.090	0.301	0.303	0.396	1002.88	0.144	0.184	0.030	0.642
3000_100%_9BTDC_EGR=0.2	1561.54	150.13	0.096	213.528	13.113	13.321	17.072	43.506	0.301	0.306	0.392	1154.37	0.096	0.137	0.028	0.739
3000_100%_12BTDC_EGR=0	1561.54	471.46	0.302	361.204	19.926	19.509	21.168	60.603	0.329	0.322	0.349	668.27	0.302	0.231	0.039	0.428
3000_100%_12BTDC_EGR=0.1	1561.54	256.47	0.164	288.723	15.513	15.602	19.116	50.231	0.309	0.311	0.381	966.12	0.164	0.185	0.032	0.619
3000_100%_12BTDC_EGR=0.2	1561.54	174.77	0.112	215.842	14.178	14.369	17.428	45.975	0.308	0.313	0.379	1124.95	0.112	0.138	0.029	0.720
3000_100%_15BTDC_EGR=0	1561.54	489.69	0.314	348.312	21.658	21.150	20.774	63.582	0.341	0.333	0.327	659.95	0.314	0.223	0.041	0.423
3000_100%_15BTDC_EGR=0.1	1561.54	284.41	0.182	287.478	16.939	16.987	19.351	53.278	0.318	0.319	0.363	936.37	0.182	0.184	0.034	0.600
3000_100%_15BTDC_EGR=0.2	1561.54	197.62	0.127	219.012	15.494	15.662	17.711	48.867	0.317	0.320	0.362	1096.04	0.127	0.140	0.031	0.702
3000_100%_18BTDC_EGR=0	1561.54	484.95	0.311	351.157	23.426	22.830	20.499	66.755	0.351	0.342	0.307	658.68	0.311	0.225	0.043	0.422
3000_100%_18BTDC_EGR=0.1	1561.54	313.41	0.201	284.854	18.769	18.754	19.446	56.968	0.329	0.329	0.341	906.31	0.201	0.182	0.036	0.580
3000_100%_18BTDC_EGR=0.2	1561.54	191.74	0.123	196.474	15.070	15.284	16.608	46.962	0.321	0.325	0.354	1126.36	0.123	0.126	0.030	0.721